THE GEOLOGICAL SOCIETY OF AMERICA®

Underthrusting and duplexing beneath the northern Tibetan Plateau and the evolution of the Himalayan-Tibetan orogen

Andrew V. Zuza[1,*], Chen Wu[2], Zengzhen Wang[3], Drew A. Levy[1], Bing Li[3], Xiaosong Xiong[4], and Xuanhua Chen[3]
[1]NEVADA BUREAU OF MINES AND GEOLOGY, UNIVERSITY OF NEVADA, RENO, NEVADA 89557, USA
[2]STRUCTURAL GEOLOGY GROUP, CHINA UNIVERSITY OF GEOSCIENCES (BEIJING), BEIJING 100083, CHINA
[3]INSTITUTE OF GEOMECHANICS, CHINESE ACADEMY OF GEOLOGICAL SCIENCES, BEIJING 100037, CHINA
[4]INSTITUTE OF GEOLOGY, CHINESE ACADEMY OF GEOLOGICAL SCIENCES, BEIJING 100037, CHINA

ABSTRACT

The Cenozoic Qilian Shan thrust belt is the northern margin of the Tibetan Plateau, which developed in part due to progressive India-Asia convergence during Himalayan-Tibetan orogeny. Available geologic observations suggest that this thrust belt started deforming shortly after initial India-Asia collision at 60–55 Ma, and thus its kinematic development is intrinsically related to the construction and evolution of the Tibetan Plateau. Here, we present new field observations from a geologic traverse across the Qilian Shan to elucidate the style of deformation across the active thrust belt. In particular, we infer protracted out-of-sequence deformation here that is consistent with this thrust system remaining a stationary northern boundary to the Tibetan Plateau since the early Cenozoic. We present a lithosphere-scale model for this region that highlights the following: (1) coupled distributed crustal shortening and underthrusting of the North China craton beneath Tibet, which explains the spatial and temporal distribution of observed crustal shortening and thickness, (2) this underthrusting exploited the south-dipping early Paleozoic Qilian suture paleo–subduction mélange channel, and (3) development of a lower-crustal duplex at the lithospheric underthrusting ramp. This last inference can explain the relatively high elevation, low relief, and thickened crust of the central Qilian Shan, as well as the comparative aseismicity of the region, which experiences fewer earthquakes due to less upper-crustal faulting. Both the northern and southern margins of the Himalayan-Tibetan orogen appear to have developed similarly, with continental underthrusting and crustal-scale imbrication and duplexing, despite vastly different climatic and plate-velocity boundary conditions, which suggests that the orogen-scale architecture of the thrust belt is controlled by neither of these forcing mechanisms. Instead, strength anisotropies of the crust probably control the kinematics and style of deformation, including the development of northern Tibet, where thrust systems are concentrated along pre-Cenozoic suture zones.

LITHOSPHERE; v. 11; no. 2; p. 209–231 | Published online 20 December 2018 https://doi.org/10.1130/L1042.1

INTRODUCTION

How the Tibetan crust accommodates India-Asia convergence and deforms to develop the Tibetan Plateau are outstanding questions in the study of the Himalayan-Tibetan orogen (e.g., Yin and Harrison, 2000; Clark and Royden, 2000; Tapponnier et al., 2001; van Hinsbergen et al., 2011a, 2011b; Yakovlev and Clark, 2014; Ingalls et al., 2016; Zheng et al., 2017). The evolution of the Tibetan Plateau directly impacts our knowledge of continental tectonics (Molnar, 1988; Yin, 2010), and examination of the northernmost margin of the Tibetan Plateau is key to unravelling the deformation mechanisms acting in northern Tibet (Fig. 1). Since the 1970s (Dewey and Burke, 1973; Molnar and Tapponnier, 1975), intense study of the Tibetan Plateau has led to a series of end-member models for its formation, including: (1) Cenozoic vertically coherent shortening of the Tibetan lithosphere (England and Houseman, 1986; Dewey et al., 1988), (2) Cenozoic underthrusting of the Asian lithosphere beneath the Tibetan Plateau (Willett and Beaumont, 1994; Kind et al., 2002; Zhou and Murphy, 2005; Zhao et al., 2011; Feng et al., 2014; Ye et al., 2015), (3) Cenozoic vertical inflation of Tibetan crust by lateral channel flow (Zhao and Morgan, 1987; Bird, 1991; Royden et al., 1997, 2008; Clark and Royden, 2000), (4) discrete Cenozoic intracontinental subduction coupled with lateral extrusion along major strike-slip faults (Tapponnier et al., 2001), (5) Cenozoic uplift of the central plateau via shortening and mantle processes (e.g., England and Houseman, 1989; Harrison et al., 1992; Molnar et al., 1993), followed by outward plateau expansion to the north, east, and south (Wang et al., 2008), and (6) pre-Cenozoic crustal thickening (e.g., Worley and Wilson, 1996; Murphy et al., 1997; Wallis et al., 2003; see Fig. 2). An important difference between many of these models is the way in which the continental crust and mantle lithosphere accommodate the convergence between India and Asia, and the degree of coupling between these two layers (e.g., Willett and Beaumont, 1994).

These tectonic models make specific predictions for the timing of deformation, location and kinematics of crustal structures, and the strain distribution in northern Tibet (e.g., Meyer et al., 1998; Lease et al., 2012; Zuza et al., 2016a). Thus, systematic geological observations ranging from

Andrew V. Zuza http://orcid.org/0000-0001-6130-5121
*azuza@unr.edu; avz5818@gmail.com

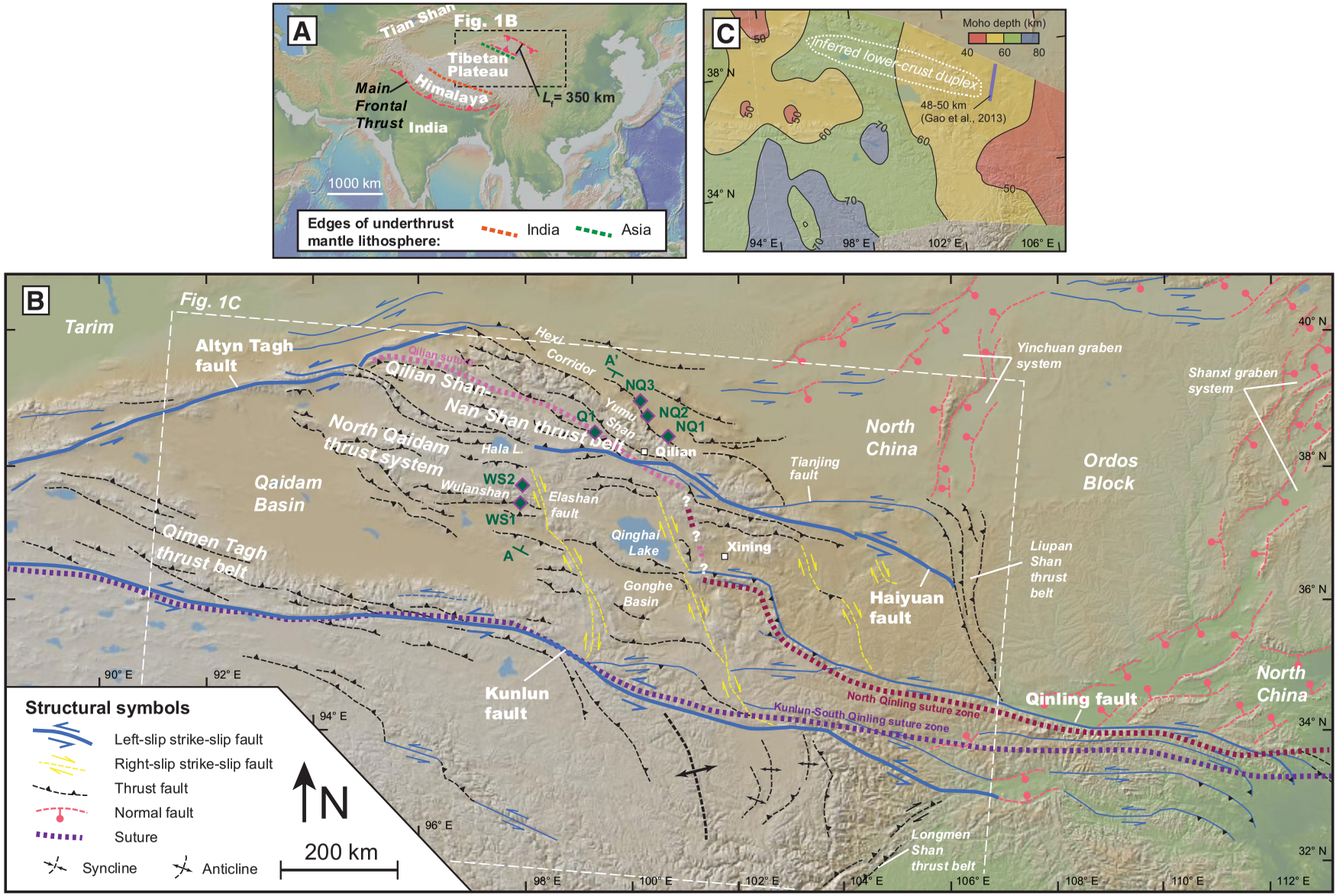

Figure 1. (A) Map of the Himalayan-Tibetan orogen showing the location of Figure 1B. The northern edge of Indian lithosphere is from Nábelek et al. (2009) and the southern edge of Asian lithosphere is from Ye et al. (2015). (B) Map of Cenozoic faults in northern Tibet based on Burchfiel et al. (1991), Gaudemer et al. (1995), Taylor and Yin (2009), Gao et al. (2013), and Zuza et al. (2016a). Also shown is approximate cross-section line A-A′ for Figure 9. Annotations NQ1, NQ2, NQ3, Q1, WS1, and WS2 correspond to field sites discussed in this study. (C) Contoured crustal thickness estimates derived from receiver-function analysis of Yue et al. (2012). Seismic-reflection cross-section line and Moho depth are from Gao et al. (2013). Dashed white line is the approximate location of inferred lower-crustal duplexing.

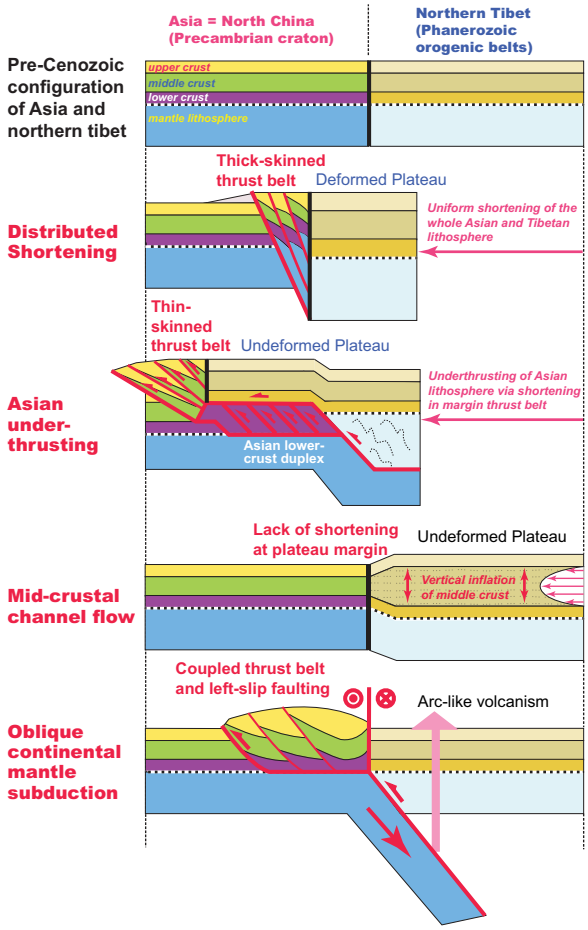

Figure 2. End-member models for the development of the northern Tibetan Plateau.

surface geology to deep-crustal seismic images can help to distinguish the dominant deformational process acting along the northern margin of the Tibetan Plateau. The last few decades have witnessed prolific research across northern Tibet, including geophysical studies, low-temperature thermochronology analyses, and field-based mapping investigations. In this contribution, we review these studies and present new field observations from a transect across the Qilian Shan thrust belt to provide an updated synthesis on the style, magnitude, and timing of continental deformation related to the growth of the northern Tibetan Plateau.

We integrated surface geologic data from mapping traverses across the Qilian Shan with available geophysical data sets to document the development of the northern margin of the Tibetan Plateau. The inference that Cenozoic deformation initiated here shortly after India-Asia collision in the Eocene (e.g., Clark et al., 2010; Yin et al., 2008a, 2008b; Duvall et al., 2011; Clark, 2012; Qi et al., 2016; Yu et al., 2017) and is still active today requires that thrusting has been out-of-sequence for much of the Cenozoic (e.g., Jolivet et al., 2001; George et al., 2001). We present field evidence for this out-of-sequence faulting across much of the Qilian Shan, from the North Qilian Shan frontal thrusts in the north to the Wulanshan thrust system, which defines the southern extent of the Qilian Shan. In addition, based on the location and geometry of Miocene and younger shortening, present-day seismicity, and geomorphology and topography across the Qilian Shan, we suggest that duplexing and accretion of the middle-to-lower crust were at least partially responsible for thickening the crust in the central Qilian Shan. Furthermore, crustal thickening via this accretion may have induced widespread strike-slip faulting in the middle Miocene (Fig. 3; e.g., Duvall et al., 2013; Yuan et al., 2013).

GEOLOGIC SETTING

Himalayan-Tibetan Orogen

The Cenozoic Himalayan-Tibetan orogen resulted from the collision of the Indian and Asian plates (e.g., Yin and Harrison, 2000; Royden et al., 2008) at 60–55 Ma (see recent discussions in DeCelles et al., 2014; Hu et al., 2015, 2016). The orogen has a north-south width (i.e., nearly convergence-parallel direction; Zhang et al., 2004) of >2000 km, from the Himalayan fold-thrust belt in the south to the Qilian Shan thrust belt in north (Fig. 1). Most of the present-day topography, crustal thickness, and presently active structures were generated during India-Asia collision (e.g., Yin and Harrison, 2000; Tapponnier et al., 2001; Royden et al., 2008), although there are notable exceptions of inherited crustal thickness and structures as documented for the southern and eastern portions of Tibet (e.g., Worley and Wilson, 1996; Murphy et al., 1997; Kapp et al., 2003, 2007; Robinson et al., 2004; Tian et al., 2016). That said, preexisting structures often control the distribution of Cenozoic deformation, including the Paleozoic–Mesozoic suture zones across Tibet (e.g., Yin and Harrison, 2000; Wu et al., 2016, 2017; Zuza et al., 2018).

The Tibetan Plateau is bounded by the northeast-striking left-slip Altyn Tagh fault in the northwest and three other thrust systems: the west-northwest-trending Himalaya to the south, the northwest-trending Qilian Shan in the northeast, and the north-trending Longmen Shan in the east (Fig. 1). A cross section across the Tibetan Plateau parallel to India-Asia convergence involves the Himalaya to the south and the Qilian Shan to the north, and thus an understanding of the kinematics and/or dynamics of the Tibetan Plateau requires comprehensive knowledge of the structural framework of these two distinct thrust systems. Investigations across the Himalaya have been robust (e.g., Burchfiel et al., 1995; Johnson, 2002; DeCelles et al., 2002; Robinson et al., 2006; McQuarrie et al., 2008; Webb et al., 2011, 2017; Webb, 2013; Gao et al., 2016; and many others), and our knowledge of Cenozoic crustal deformation across the northern plateau margin is growing (e.g., Gaudemer et al., 1995; Meyer et al., 1998; Lease et al., 2012; Gao et al., 2013; Craddock et al., 2014; Cheng et al., 2015; Zuza et al., 2016a, 2017a, 2018; Allen et al., 2017; Yu et al., 2017). Herein, discussion of this orogen is concerned primarily with the geology of northern Tibet, north of the Kunlun left-slip fault (Fig. 1).

Geology of Northern Tibet

The northeastern Tibetan Plateau has an average elevation of ~4.5 km, and this high topography decreases rapidly to <1.5 km in the Hexi Corridor foreland basin to the north (Fig. 1). Geophysical observations show that the crust is locally 55–65 km thick (Zhao et al., 2001; Yue et al., 2012; Gao et al., 2013; Xu et al., 2018), and the relatively stable crust beneath Ordos Basin to the north is ~42 km thick (Fig. 1; Liu et al., 2006; Pan and Niu, 2011).

The northern boundary of the Tibetan Plateau is presently the Qilian Shan–Nan Shan thrust belt and left-slip Haiyuan fault (Fig. 1; e.g., Burchfiel et al., 1991; Zhang et al., 1991; Gaudemer et al., 1995; Yin and Taylor, 2009; Guo et al., 2016). These Cenozoic features overprint complex geological relationships that include early Paleozoic orogeny and Mesozoic extension, which we briefly discuss below (e.g., Xiao et al., 1974; Wang and Liu, 1981; Yin and Harrison, 2000; Xiao et al., 2009; Xia and Song, 2010; Song et al., 2013).

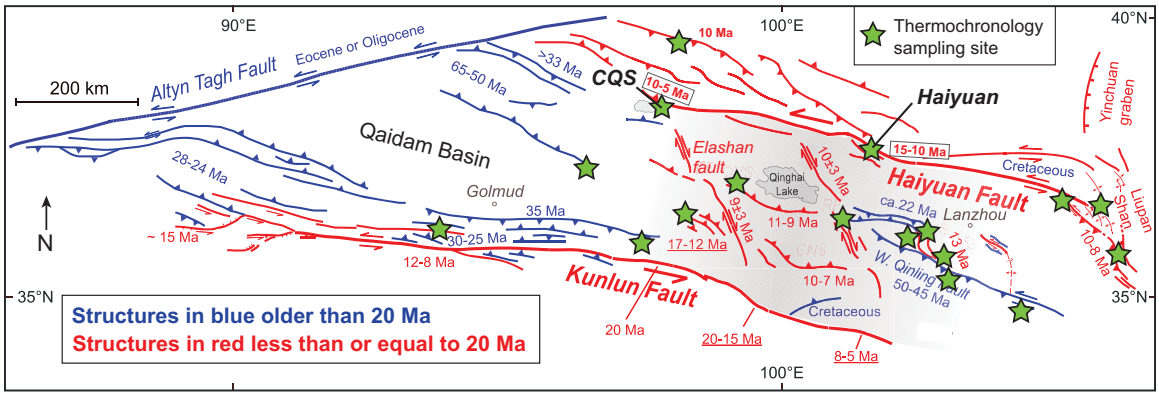

Figure 3. Inferred ages of major Cenozoic structures across northern Tibet based on thermochronology data (shown with green stars). Figure is modified from Duvall et al. (2013) and Yuan et al. (2013), and cooling ages come from a variety of sources discussed in the text. Also included are our reconnaissance thermochronology investigations at the Central Qilian Shan (CQS) and Haiyuan sites (Zuza et al., 2016b; Li et al., 2019).

Paleozoic Geology

The early Paleozoic Qilian orogen, as summarized by Song et al. (2013) and Zuza et al. (2018), involved the collision of the Proterozoic Qaidam microcontinent with the Archean–Proterozoic North China craton to the north in the Ordovician–Silurian. Widespread Cambrian–Ordovician arc volcanic and plutonic rocks represent the Qilian arc, which accommodated the convergence between these two continents (Wu et al., 2017) and the closure of the Qilian ocean, although the number and polarity of these subduction systems are debated (e.g., Xiao et al., 2009; Song et al., 2013; Zuza and Yin, 2017; Zuza et al., 2018). Dismembered mélange-ophiolite complexes are found throughout the Qilian Shan, and they represent the Qilian suture(s) (Yin and Harrison, 2000; Yin et al., 2007b; Menold et al., 2009, 2016; Song et al., 2013, 2014).

As previously outlined in Zuza et al. (2018), we believe the simplest model that explains available field observations involves a single south-dipping subduction system that was constructed along the northern margin of the Qaidam continent, as originally described and discussed by Sobel and Arnaud (1999) and Gehrels et al. (2003a, 2003b). Subsequent contractional deformation during early Paleozoic Qilian and Cenozoic Himalayan-Tibetan orogenies reorganized the original tectonic configuration of the early Paleozoic Qilian arc, leading to an apparent multitude of suture zones (e.g., Xiao et al., 2009; Yin et al., 2007b). Qilian orogeny ceased by the Devonian, and Carboniferous strata were deposited unconformably over amphibolite-grade arc and basement rocks (Xiao et al., 2009; Wu et al., 2017).

Mesozoic Geology

Jurassic and Cretaceous extensional and transtensional basin deposits are observed across northern Tibet and the Qilian Shan, from Xining Basin in the south to the Hexi Corridor in the north (Horton et al., 2004; Pan et al., 2004). These deposits have been related to the Mesozoic closure of the Paleo-Tethys and Meso-Tethys Oceans south of Qaidam Basin (Pullen et al., 2008; Zhang et al., 2014), and associated slab rollback to the south may have led to regional extension that affected much of the continent to the north (Huo and Tan, 1995; Vincent and Allen, 1999; Chen et al., 2003; Yin et al., 2008a, 2008b). Extensional faults and related basins have been imaged in the upper crust via seismic profiling (Yin et al., 2008a, 2008b). Although there are extensive Jurassic and Cretaceous strata and basin deposits, actual Mesozoic normal faults are rarely exposed in the field (e.g., Chen et al., 2014; Cheng et al., 2019). As discussed later, Mesozoic normal faults do not appear to be significantly reactivated by Cenozoic thrusting in either seismic images or field observations.

Cenozoic Geology

The major Cenozoic thrust belts in northern Tibet are the Qilian Shan, North Qaidam, Qaidam Basin, and Qimen Tagh (Eastern Kunlun Shan), from north to south, respectively (Fig. 1; Gaudemer et al., 1995; Jolivet et al., 2003; Yin et al., 2007a, 2008a, 2008b; Cheng et al., 2014). These thrust systems appear to be kinematically linked with the active >1000-km-long, east-striking Haiyuan, Qinling, and Kunlun left-slip faults (Fig. 1; e.g., Taylor and Yin, 2009; Zuza and Yin, 2016). For example, the left-slip Haiyuan fault terminates to the west within the Qilian Shan, just north of Hala Lake (Fig. 1), and the left-slip Kunlun fault appears to die out within the Qimen Tagh thrust belt, to the south of Qaidam Basin (Fig. 1). The strike-slip faults are lithospheric structures (Wang et al., 2011; Gao et al., 2013) that parallel the surface traces of the Paleozoic and Mesozoic Qilian, Qinling, and Kunlun sutures (Fig. 1; Yin and Harrison, 2000; Wu et al., 2016). These aforementioned west-northwest–striking thrust belts and strike-slip faults are obliquely oriented to the northeast-striking left-slip Altyn Tagh fault (Fig. 1; e.g., Yue et al., 2001; Yin et al., 2002; Cowgill, 2007).

These thrust belts accommodated significant Cenozoic shortening across northern Tibet (e.g., Gaudemer et al., 1995; Meyer et al., 1998; Wang and Burchfiel, 2004; Yin et al., 2007a, 2007b, 2008a, 2008b; Zheng et al., 2010; Cheng et al., 2015; Allen et al., 2017; Yang et al., 2018; see also Fig. 1). A synthesis of shortening estimates suggests a minimum of 250–350 km of Cenozoic north-south shortening, which equates to 40%–45% shortening strain across the ~400-km-wide region encompassing Qaidam Basin to the Hexi Corridor (Zuza et al., 2016a, 2018). Cheng et al. (2015) similarly documented ~250 km of shortening based on a mass balance of ~360 km of left-slip offset on the Altyn Tagh fault accommodated by shortening within the Qilian Shan. Less is known about the Qimen Tagh or Eastern Kunlun Shan (Fig. 1) south of Qaidam Basin, although Yin et al. (2007a, 2008b) documented >30 km of shortening (>30% strain) across some of the northern ranges of the Qimen Tagh thrust system.

Geodetic and geologic evidence suggests that northern Tibet has experienced clockwise rotation throughout much of the Cenozoic. Multiple balanced cross section constructed across the Qaidam Basin thrust belt (Fig. 1) indicate an eastward decrease in north-south Cenozoic shortening

(Yin et al., 2008a, 2008b; Wei et al., 2016). A similar eastward decrease in Cenozoic shortening strain may be inferred across the Qilian Shan–Nan Shan and Qimen Tagh thrust belts on the basis of an eastward decrease in the (1) number of thrusts, (2) thrust belt width, and (3) average elevation (Fig. 1). An eastward-decreasing strain gradient implies clockwise rotation across northern Tibet. Paleomagnetic observations also suggest 15°–20° of total clockwise rotation across northern Tibet with respect to the Eurasian reference pole since the Cretaceous at a rate of ~0.3–0.5°/m.y. (Frost et al., 1995; Halim et al., 1998, 2003; Cogné et al., 1999; Dupont-Nivet et al., 2004; Chen et al., 2002a, 2002b; Sun et al., 2006).

Over the past two decades, significant advancements have been made to unravel deformation timing and rates via sedimentological and low-temperature thermochronological analyses. Regionally, it is apparent that Cenozoic deformation started by 55–40 Ma and accelerated at 20–15 Ma (e.g., Bovet et al., 2009; Yuan et al., 2013; Duvall et al., 2013; Craddock et al., 2014; Zhuang et al., 2018; Jian et al., 2018). Thrusting initiated locally at 50–45 Ma in the southern Qilian Shan and North Qaidam thrust belts, and deformation migrated southward to the Qimen Tagh and northward to the northern Qilian Shan thrust belts by 25–20 Ma (Fig. 3; Mock et al., 1999; Jolivet et al., 2001; Dupont-Nivet et al., 2004; Horton et al., 2004; Yin et al., 2008a, 2008b; Clark et al., 2010; Duvall et al., 2011; Baotian et al., 2013; Qi et al., 2016; Zheng et al., 2017; Ji et al., 2017; Yu et al., 2017; Jian et al., 2018).

Starting at 20–15 Ma, northern Tibet experienced a pulse of rapid cooling and exhumation that overlapped with the through-going initiation of the major left-slip Kunlun, Qinling, and Haiyuan faults (Fig. 3; e.g., Jolivet et al., 2001; Craddock et al., 2011; Duvall et al., 2013; Yuan et al., 2013; Zuza et al., 2016b; Li et al., 2019). Here, we note that although left-slip strike-slip faulting is inferred to have begun at ca. 20–15 Ma in northern Tibet, there are relatively few age constraints for strike-slip fault initiation, especially along the Haiyuan fault (Fig. 3; e.g., Yuan et al., 2013; Duvall et al., 2013). Recent apatite (U-Th)/He and fission-track (AFT) analyses across a restraining bend of the Haiyuan fault at 37.6012°N and 101.5468°E suggest that rapid exhumation inferred to be related to Haiyuan fault motion occurred at ca. 15–10 Ma (Li et al., 2019), which is consistent with previously proposed initiation ages for the Haiyuan fault (Fig. 3; see summary in Duvall et al., 2013).

KINEMATICS OF THE TIBETAN PLATEAU'S NORTHERN MARGIN

We modeled shortening rate, crustal thickening, and elevation changes through time across the northern Tibet region using external convergence-rate constraints across the entire Himalayan-Tibetan orogen. The goal of this exercise was to generate simple shortening strain predictions to compare against shortening observations from our own work and published data. More specifically, the simple observation that convergence rates across the Himalayan-Tibetan orogen have decreased since initial collision at ca. 58 Ma (Molnar and Tapponnier, 1975; Molnar and Stock, 2009; Copley et al., 2010; DeCelles et al., 2014; Hu et al., 2016) effectively requires shortening rates across the intraplateau thrust belts to have fluctuated accordingly. That is, shortening rates probably decreased through time, although we note that variable strain partitioning among thrust belts may have led to more complex shortening-rate relationships. Therefore, we attempted to provide some external bounds for comparison with field-based shortening data. The present-day north-northeast-directed convergence rate across the Qilian Shan thrust system is 5–7 mm/yr (Zhang et al., 2004; Gan et al., 2007). Here, we take the approach of applying an orogen-scale bulk strain rate—which is inferred to have remained constant throughout the Cenozoic (Clark, 2012)—to northern Tibet to estimate bounds on local deformation magnitude and rate. This approach assumes that the northern boundary of the Himalayan-Tibetan orogen has remained stationary with time (Clark, 2012).

The velocity field across the Himalayan-Tibetan orogen yields an orogen-scale bulk strain rate ($\dot{\varepsilon}$) of 6.6×10^{-16} s^{-1} (i.e., the rate of change of the orogen's width divided by its width, ~40 mm yr^{-1}/~1900 km; Fig. 1; Clark, 2012). The strain rate at the time of collision can be estimated using plate-circuit reconstructions for the India-Asia convergence rate at the time of collision (ca. 58 Ma) and the estimated orogen width derived from these reconstructions (Molnar and Stock, 2009; van Hinsbergen et al., 2011a, 2011b; Huang et al., 2017): At ca. 58 Ma, the convergence rate and orogen width were ~120 ± 10 mm/yr and 6050 ± 450 km, respectively, which yields a bulk strain rate of $6.3 \pm 0.9 \times 10^{-16}$ s^{-1}. This value overlaps the present-day strain rate of 6.6×10^{-16} s^{-1} (Clark, 2012). This rate applied to the Qilian Shan thrust belt can be used to estimate shortening rate and magnitude through time according to the following relationships (Clark, 2012; Zuza et al., 2017b):

$$x(t) = L_f\left(e^{-\dot{\varepsilon}t} - 1\right), \quad (1)$$

$$L(t) = L_f e^{-\dot{\varepsilon}t}, \quad (2)$$

$$v\left(x = L(t)\right) = \dot{\varepsilon} L_f e^{-\dot{\varepsilon}t}, \quad (3)$$

where $L(t)$ is the width of the orogen at time t (where $t = 0$ m.y. is today, and $t = -58$ m.y. is the time of collision), L_f is the final width of the orogen or $L(t = 0$ m.y.), $x(t)$ is the width of a deforming segment of the orogen, such that $x(t) + L_f = L(t)$, and $v(x)$ is the rate at which a point at position x moves north toward stable Eurasia and is the orogen-scale convergence rate at $x = L(t)$. Total shortening is defined by $L(t = -58$ m.y.) minus L_f. We assumed the final length of this region (i.e., from the northernmost Qaidam Basin to the southernmost Hexi Corridor; Fig. 1) was ~350 km. We also assumed that most of the crust was ~35 km thick prior to the Cenozoic, which we justify because: (1) the relatively undeformed Ordos Basin to the north is ~42 km thick (Liu et al., 2006), and (2) modern extended or rifted continental crust thickness is between 30 and 40 km thick (Christensen and Mooney, 1995), which applies to northern Tibet following Mesozoic extension (Vincent and Allen, 1999). Note that this analysis assumes plane-strain deformation, where "extrusion"-type processes are not accounted for (e.g., Tapponnier et al., 1982; Cheng et al., 2015).

In Figure 4A, we plot shortening rate and magnitude over a range of constant strain rates from 5×10^{-16} s^{-1} to 7×10^{-16} s^{-1}, assuming either (1) deformation initiated at ca. 58 Ma, or (2) alternatively, deformation started at ca. 40 Ma, as geologic evidence suggests (e.g., Craddock et al., 2011). If the initiation timing is between these values, one can extrapolate between the curves (Fig. 4A). To further demonstrate parameter sensitivity in our model, we modeled two L_f values: 350 km and 300 km. For the purposes of this discussion, we primarily use the ca. 40 Ma initiation age for deformation. Using this time and assuming pure-shear crustal thickening, isostatic compensation, a total ~5 km of erosion, and a constant 6.6×10^{-16} s^{-1} strain rate, Figure 4B shows the expected crustal thickening and elevation through time. We also plotted the modeled elevation through time of the Qaidam Basin from Yu et al. (2015), which assumes that basin sedimentation leads to crustal uplift following isostasy (Fig. 4B). Note that the Qilian Shan elevation remains at or higher than the estimated elevation of Qaidam Basin, which is required for continuous Cenozoic Qilian Shan–derived sedimentation into the basin and for the Qilian Shan to trap sediments in the endorheic basin (Yu et al., 2015).

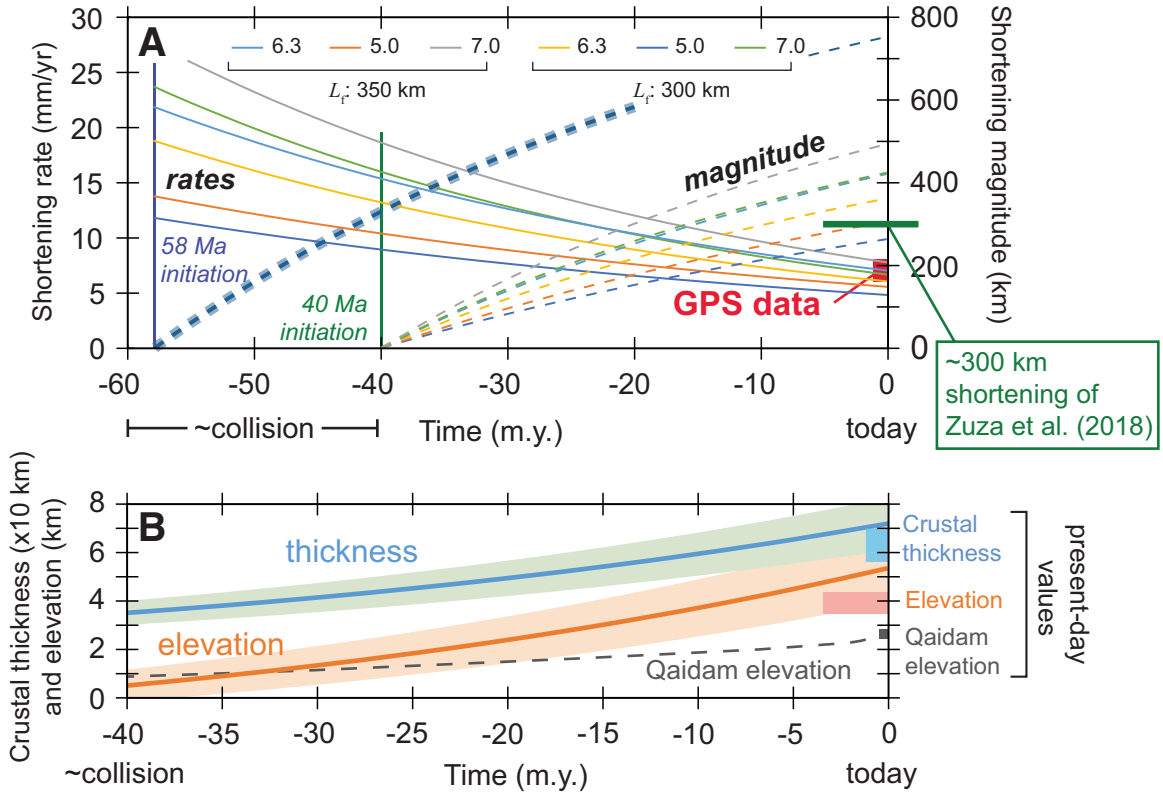

Figure 4. (A) Time-varying shortening rate and magnitude across the Qilian Shan assuming strain rates ranging from 5 × 10^{-16} s^{-1} to 7 × 10^{-16} s^{-1}. Curves correspond to different strain rates, ×10^{-16} s^{-1}. Two L_f values were also modeled to demonstrate model variability. Shortening magnitude curves were primarily modeled assuming shortening initiation at ca. 40 Ma, consistent with geological observations, but the thick blue dashed line shows expected shortening magnitude assuming ca. 58 Ma initiation. Global positioning system (GPS) data are from Gan et al. (2007). (B) Modeled crustal thickness starting with initially 35-km-thick crust subjected to the shortening in Figure 4A (using 6.3 × 10^{-16} s^{-1} strain rate) and predicted elevation following this crustal thickening, given isostasy. Plotted for reference is a curve of Qaidam Basin elevation from Yu et al. (2015). Note that the elevation of the Qilian Shan should be higher than Qaidam Basin throughout the Cenozoic to provide a continuous source of sediments for the basin and to trap its sediments and flow. Model forces ~5 km of erosion. Initial ~5 km uncertainties on crustal thickness were propagated through both as the uncertainty bounds. Present-day crustal thickness is from Yue et al. (2012).

These models, which are only based on external kinematic constraints and not on our geologic observations, predict that shortening rates have decreased from ~16 mm/yr in the Eocene at ca. 40 Ma to the present-day value of ~6 mm/yr, which matches global positioning system (GPS)–based estimates (Fig. 4A; Zhang et al., 2004). The model predicts that shortening magnitude increases to 400–450 km over a 40 m.y. period. These values are slightly higher than existing minimum shortening magnitude estimates across the thrust system (i.e., 250–350 km; Zuza et al., 2018). Both crustal thickness and elevation increase through time to reasonable estimates of 70 km and ~5 km (Fig. 4B), respectively, which is comparable to present-day values (Fig. 1).

FIELD OBSERVATIONS

Detailed field observations and mapping across the central Qilian Shan have previously been reported in Zuza et al. (2018) and Wu et al. (2017). This present study focused on new study sites along the southern and northern margins of the Qilian Shan–Nan Shan thrust belt. Specifically, our observations focused on the Wulanshan (also referred to as the Zongwulong Mountains; Yu et al., 2017), which bounds the Qilian Shan thrust belt to the south, the central thrust belt near the city of Qilian, and the northern range-front thrust system (Fig. 1). By focusing on these three locations, the goal was to relate Cenozoic deformation across the entire width of the Qilian Shan–Nan Shan thrust belt to provide an integrated view of the development of the northern margin of the Tibetan Plateau. Unit age assignments used here come from existing geologic maps, including those from Pan et al. (2004), Gansu Geological Bureau (1989), and Qinghai BGMR (1991). We did not attempt to date or confirm stratigraphic age assignments, but in the past we have found that previous ages of Paleozoic–Mesozoic units are generally accurate and have been corroborated by detrital zircon maximum depositional ages (e.g., Wu et al., 2016, 2017; Zuza et al., 2018).

North Qilian Shan

The North Qilian Shan defines the northernmost extent of the Tibetan Plateau. The predominantly north-directed North Qilian thrust system places Proterozoic–Paleozoic–Mesozoic strata over Cenozoic basin deposits of the Hexi Corridor (Li and Yang, 1998; Zhuang et al., 2011; Zheng et al., 2010; Yang et al., 2018). Typically, one major north-directed thrust

system bounds the northern extent of the North Qilian Shan (e.g., Yang et al., 2007; Zheng et al., 2010; Yang et al., 2018), with some prominent exceptions, such as the Yumu Shan (e.g., Tapponnier et al., 1990), which is a diverging fault splay of the main North Qilian Shan thrust. The Hexi Corridor foreland basins to the north of these thrusts are variably deformed by discrete south-directed back-thrust systems to the north, off of the Tibetan Plateau.

Geologic mapping and industry seismic reflection profiles show ~6 km of Mesozoic and Cenozoic strata in the Hexi Corridor and two major south-dipping thrust fault systems (Zuza et al., 2016a). This previous study estimated a minimum of ~33 km shortening (53% strain) over a deformed section length of 29 km (Zuza et al., 2016a). Extrapolation of these estimates across the entire North Qilian Shan suggests ~50 km of shortening along the northernmost Tibetan Plateau margin.

The North Qilian range front just southeast of the Yumu Shan rises abruptly from the relatively flat Hexi Corridor (Fig. 5A). Exposure along this thrust-bounded range is often poor, but at location NQ1 in Figure 1, the major thrust fault is observed in drainages placing Carboniferous strata over Cenozoic deposits (Fig. 5B). North- and south-dipping (40°–60° dips) faults are observed in the thrust hanging wall with dip-slip striations (Fig. 5B). Despite numerous conjugate-fault sets, map-view and field relationships require north-directed thrusting of Carboniferous strata over Cenozoic foreland basin deposits (e.g., Yang et al., 2018). At another location—NQ3 in Figure 1—fault splays are observed in the footwall rocks of the North Qilian thrust system, duplicating Cenozoic strata. An ~100-m-wavelength, southeast-trending, open-close anticline is observed in the hanging wall of a minor north-directed thrust fault splay located entirely within Cenozoic strata (Fig. 5C). These observed minor faults may represent incipient range-bounding structures. Yang et al. (2018) reported that the west-trending Hujiatai anticline to the west of the Yumu Shan is shortening at a rate of 0.8 mm/yr.

Between sites NQ1 and NQ3, at site NQ2 in Figure 1, we observed an uplifted and exposed hanging wall–footwall flat structure, where Ordovician metasedimentary rocks are thrust over Cenozoic basin deposits, and this entire system is truncated by more recent higher-angle thrust faults (Fig. 6). Age constraints on these local Cenozoic sediments are lacking, but they are probably Oligocene or Miocene (Li and Yang, 1998; Pan et al., 2004; Zhuang et al., 2011; Fang et al., 2012). We infer that these exposures represent out-of-sequence deformation along the northern margin of the Tibetan Plateau, based on the following observations and logic. The horizontal contact between Ordovician strata and Cenozoic deposits is a thrust fault that is parallel to both the hanging-wall and footwall rocks (i.e., a thrust flat). This subhorizontal fault is truncated by higher-angle thrust faults that appear to be more recent because they control topography along this range front (Fig. 6). Earlier movement along the high-angle fault would have disrupted a subhorizontal thrust sheet, which would make it difficult to form the observed thrust flat. We also observed relict erosional surfaces that are subparallel to the thrust flat, but that are offset vertically from each other by >670 m by the more recent, higher-angle thrust faulting (Fig. 6A). We interpret an early-stage of thrusting that produced the thrust-flat geometries, when Ordovician strata overthrust onto early Cenozoic (e.g., Eocene–Oligocene; Li and Yang, 1998; Zhuang et al., 2011) foreland basin deposits. Sometime after this faulting, the relict erosional surfaces developed, parallel to the fault flat. More recently, these faults were crosscut by out-of-sequence thrusting by two high-angle faults: the southern one juxtaposed Ordovician rocks against Ordovician

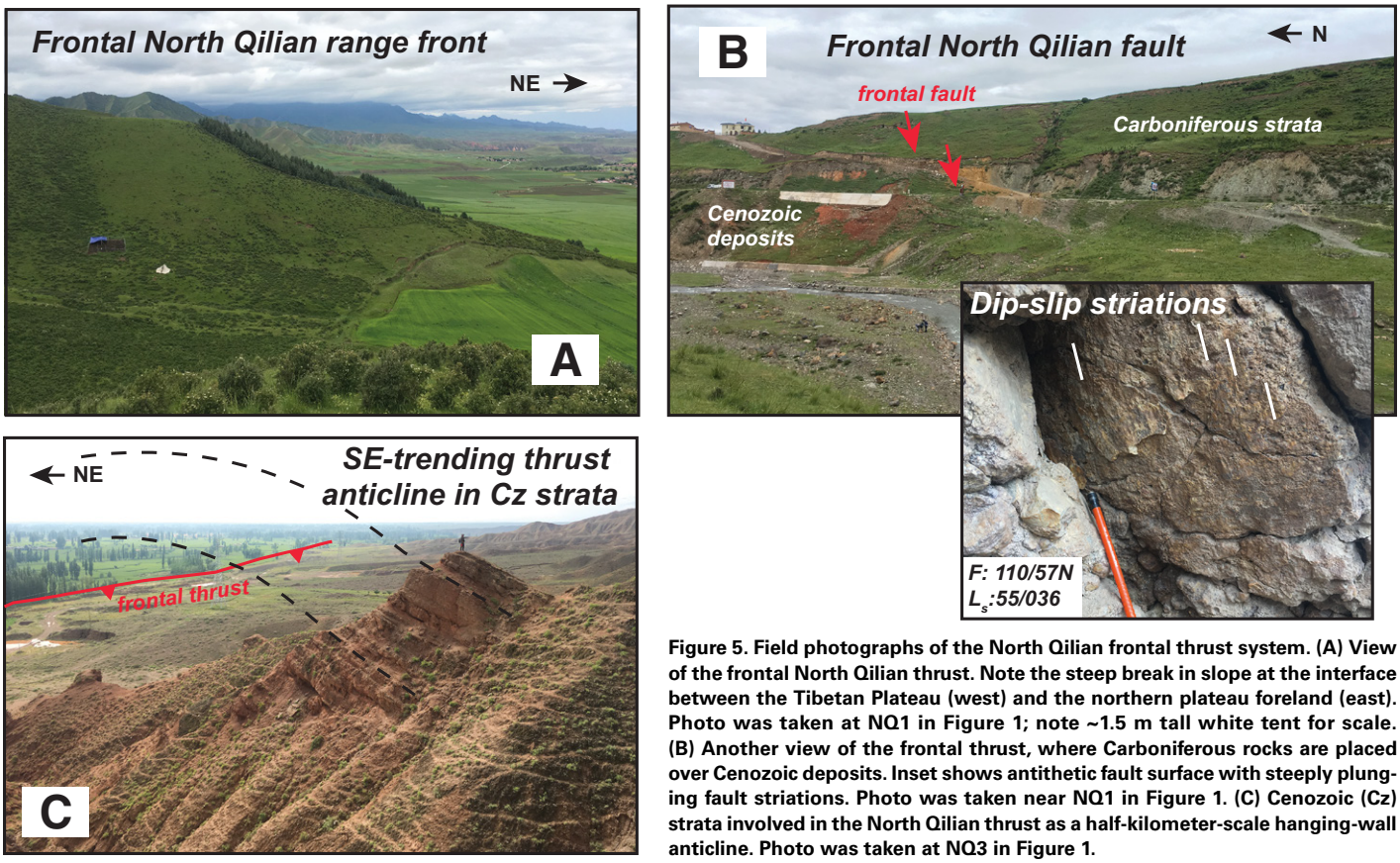

Figure 5. Field photographs of the North Qilian frontal thrust system. (A) View of the frontal North Qilian thrust. Note the steep break in slope at the interface between the Tibetan Plateau (west) and the northern plateau foreland (east). Photo was taken at NQ1 in Figure 1; note ~1.5 m tall white tent for scale. (B) Another view of the frontal thrust, where Carboniferous rocks are placed over Cenozoic deposits. Inset shows antithetic fault surface with steeply plunging fault striations. Photo was taken near NQ1 in Figure 1. (C) Cenozoic (Cz) strata involved in the North Qilian thrust as a half-kilometer-scale hanging-wall anticline. Photo was taken at NQ3 in Figure 1.

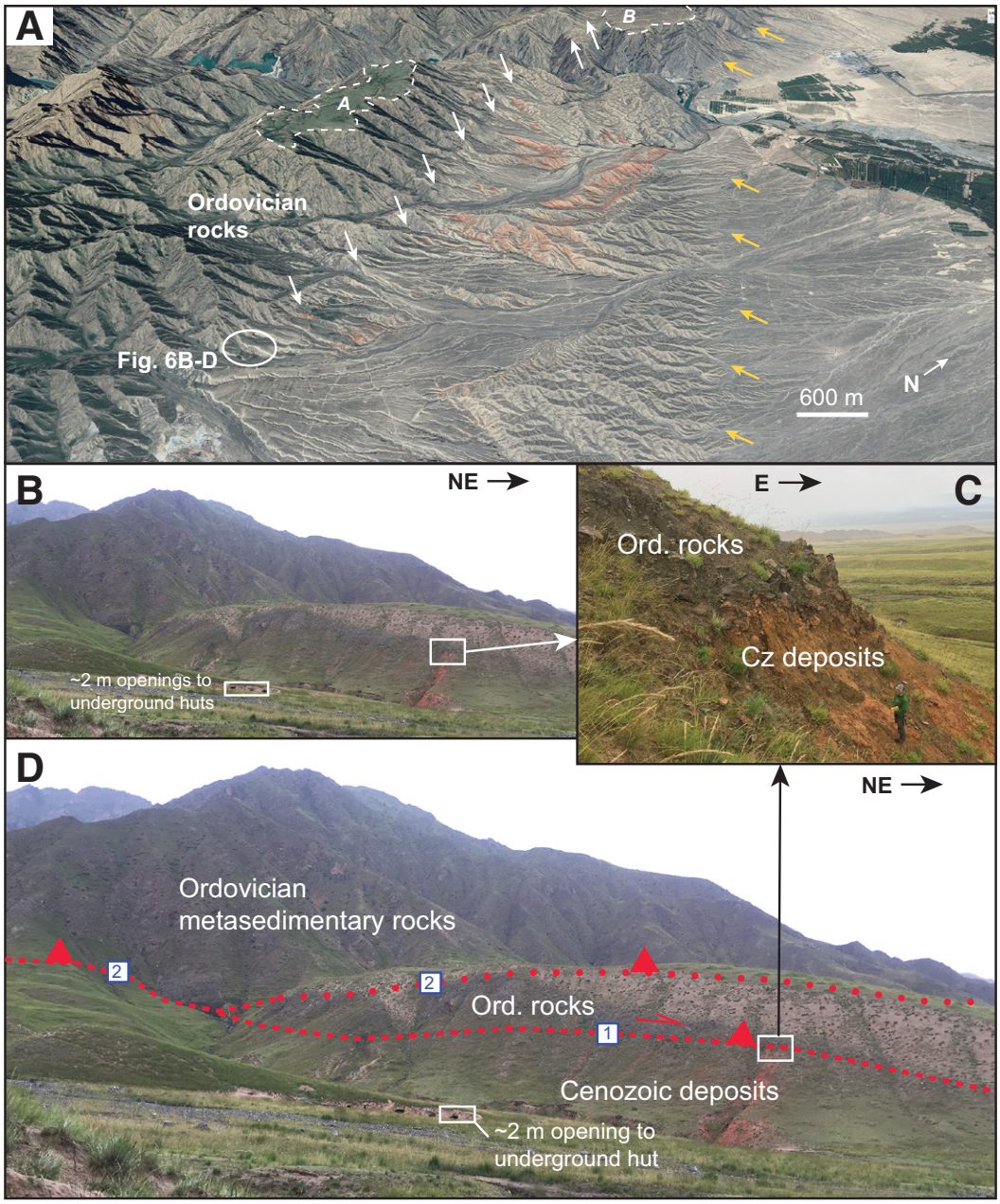

Figure 6. Satellite and field photographs of the North Qilian frontal thrust system showing exposure of out-of-sequence thrust system. Location of this site is NQ2 in Figure 1. (A) Google Earth view of the North Qilian thrust system showing two active thrust faults with white and yellow arrows. Location of Figures 6B–6D are shown with a white oval. A dashed white line outlines two relict surfaces (surfaces A and B) in Ordovician strata at different elevations that appear to have been continuous but are offset >670 m vertically by the major range-bounding thrust fault (white arrows). (B) Uninterpreted field photograph of Ordovician metasedimentary rocks thrust over Cenozoic deposits as a hanging-wall flat structure. (C) Close-up view of hanging-wall flat placing dark-colored Ordovician rocks over red-orange Cenozoic (Cz) deposits. (D) Interpretation of B, showing two faults: a hanging wall–footwall flat with Ordovician rocks over Cenozoic strata (fault 1) and the major range-bounding thrust (fault 2) that appears to truncate, or link with, fault 1. (E) Sketch of out-of-sequence geometries showing our inferred kinematics for the system; not to scale. First, Ordovician (O) rocks were emplaced over Cenozoic (Cz) deposits as part of a hanging wall–footwall flat (fault 1). Relict surfaces A and B formed after thrust emplacement and are subparallel to this flat thrust fault. Next, out-of-sequence faulting thrusted Ordovician rocks over Ordovician rocks (fault 2) as active faulting stepped toward the hinterland. This offset surfaces A and B. Another thrust fault to the east is actively uplifting the inactive fault 1 relative to the Quaternary (Q) basin in the Hexi Corridor.

rocks and uplifted the relict erosional surface, whereas the northern one placed the earlier hanging wall–footwall flat over Quaternary deposits of the Hexi Corridor (Fig. 6E).

Qilian City Ranges

Some of the best exposures of high-pressure blueschist rocks of the Qilian suture are located just west of Qilian City in the central Qilian Shan (e.g., Song et al., 2007, 2009). Here, along the east-trending Black River Valley, a belt of north-dipping, high-pressure ophiolitic mélange is observed in north-trending drainages. Other ophiolite and blueschist complexes to the southwest, including the Aoyougou and Yushigou localities (e.g., Song and Su, 1998; Xiang et al., 2007), are of similar age but dip south. Thus, we interpret the north-dipping mélange rocks near Qilian City to be the northern limb of a broad anticlinorium of the Qilian subduction complex.

Mesozoic normal faulting was directly observed in the field along the Black River (Fig. 7). Although Cretaceous basin-fill deposits related to normal faulting are prevalent in northern Tibet (e.g., Vincent and Allen, 1999), relatively few normal faults are directly observed except in seismic data (e.g., Yin et al., 2008b; Chen et al., 2014). This may suggest that many of the Mesozoic normal faults were reactivated in the Cenozoic as part of Himalayan-Tibetan orogeny. However, near Qilian City, we observed several Mesozoic normal faults that have not been reactivated by any Cenozoic contractional deformation (Fig. 7). West of Qilian City, along the Black River valley, a north-striking, dip-slip normal fault places Cretaceous strata over Ordovician metasedimentary rocks (Figs. 7 and 8C). The normal fault is orthogonal to the east-northeast–striking north-directed thrust faults that are mapped in this area, and there is no evidence for contractional deformation or reactivation (Fig. 7). Just north of Qilian City, a northwest-striking dip-slip normal fault places Cretaceous strata over Cambrian metavolcanic rocks (Fig. 7). Shear fabrics along the fault zone only show evidence for hanging-wall-down motion, and thus thrust-related reactivation seems unlikely. These observations suggest that reactivation of Mesozoic normal faults was not locally significant in the central Qilian Shan. Elsewhere across the Qilian Shan, we never see Mesozoic strata thrust over younger Cenozoic deposits (e.g., Wu et al., 2017; Zuza et al., 2018).

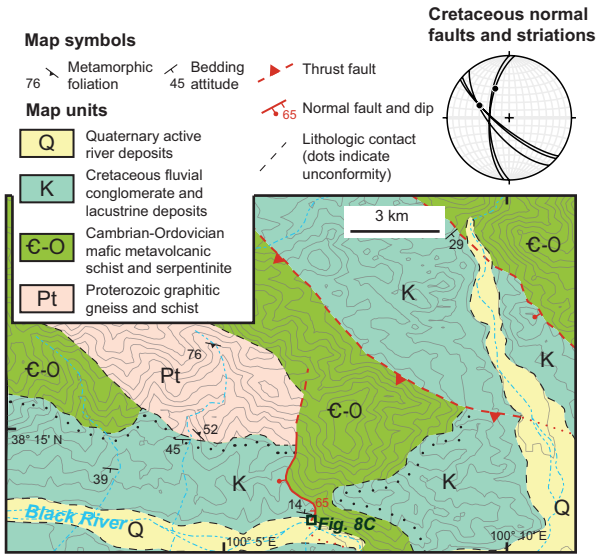

Figure 7. Geologic map along the Black River, just west of Qilian City. The normal faults are inferred to be Mesozoic, whereas the thrust fault is Cenozoic. The stereonet plots our observations of Cretaceous normal faults and striations.

About 20 km west of these localities, Mesozoic sedimentary rocks are south-dipping, and geologic maps show that these rocks were thrust northward over the Black River valley along a south-dipping hanging-wall-flat thrust fault (Fig. 8A; Gansu Geological Bureau, 1989; Pan et al., 2004). Here, Cretaceous medium-grained red-bed sandstone and pebble conglomerate rocks overlie cross-bedded, white-gray, fine- to medium-grained Triassic sandstones. The beds are subparallel. Ordovician metasedimentary rocks are thrust over, and crosscut, the package of Mesozoic strata (Figs. 8A and 8B). A north-verging hanging-wall anticline is observed, suggesting an overall hanging-wall ramp at this locality in the Ordovician rocks (Fig. 8B).

Wulanshan Thrust System

The Wulanshan thrust system, located just north of the city of Wulan to the west of Qinghai Lake (Fig. 1), represents the southernmost thrust system of the active Qilian Shan–Nan Shan thrust belt (Wang and Burchfiel, 2004). The south-directed Wulanshan is approximately correlative along-strike to the south-directed Qinghai Nanshan thrust system to the east (Craddock et al., 2014) and the Zongwulong thrust system to the west (e.g., Yu et al., 2017). The thrust-bounded ranges in the Wulanshan surround a Cenozoic basin, in which the city of Wulan is located. Well data and seismic profiles across nearby basins show that they are floored by Eocene Xiaganchaigou and Oligocene Shangganchaigou Formation rocks (Yu et al., 2017). Growth-strata relationships of the Xiaganchaigou Formation against Cenozoic thrust faults (i.e., the Olongbulak thrust) imply that deformation initiated here in the Eocene (Yu et al., 2017).

The Wulanshan range-bounding north-northeast–dipping thrust fault places Proterozoic–Paleozoic rocks over Miocene basin deposits in the Wulan Basin (e.g., Lu et al., 2012; see also Fig. 8E). Where observed, this fault and minor related fault structures dip 55°–60°N. Within the range, ~10-m-wavelength open fold pairs are observed in the Proterozoic rocks, with fold hinges parallel to the major Cenozoic range-bounding thrust fault. Although the age of this folding is not robustly constrained, based on parallelism of the fold hinge to the range-bounding thrust fault, we assume that folding also occurred in the Cenozoic. Coupled magnetostratigraphy and AFT thermochronology suggest that basin sedimentation and range uplift and exhumation, respectively, initiated at ca. 22–20 Ma (Lu et al., 2012). The Wulan sediments (Fig. 8E) were deposited between ca. 22 Ma and 9 Ma (Lu et al., 2012).

To the east, the Wulanshan thrusts are truncated and offset by the right-slip Elashan fault (Fig. 1), which has late Quaternary slip rate of ~1.1 mm/yr (e.g., Wang and Burchfiel, 2004; Yuan et al., 2011). Given that the Qinghai Nan Shan, which is truncated to the west by the Elashan fault (Fig. 1), has a very low estimated late Quaternary shortening rate of ~0.1 mm/yr (Craddock et al., 2014), we speculate that the Wulanshan accommodates higher shortening rates on the order of ~1 mm/yr. This rate is necessary to produce the observed right-lateral faulting on the Elashan fault at a rate of 1.1 mm/yr, given the fact that the right-slip fault terminates within the central Qilian Shan (Fig. 1).

The Miocene strata in Wulan Basin are variably tilted ~15–20°N (Fig. 8E; e.g., Lu et al., 2012). The most recently active thrusts crosscut and displace the Miocene sediments, and these faults are observable in satellite images parallel to the prominent range front. This relationship suggests that the active thrusting is deforming the footwall of the range-bounding thrust fault, and the thrust system is advancing to the south along this newly formed fault system. In the interior of the Wulanshan, north

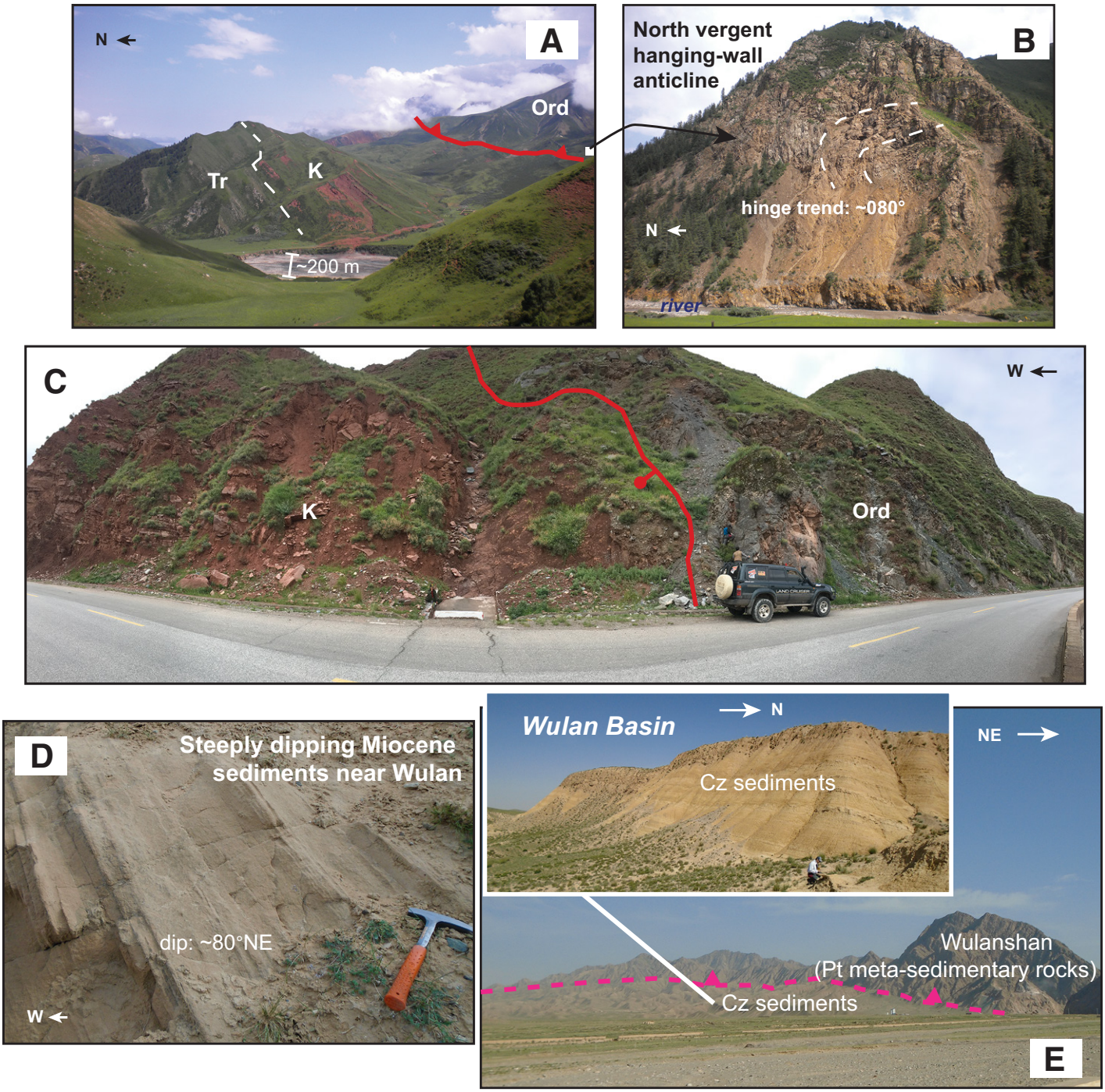

Figure 8. Field photographs from across the Qilian Shan–Nan Shan thrust system highlighting important structural relationships. (A) Ordovician rocks (Ord) are thrust northward over south-dipping subparallel Triassic (Tr)–Cretaceous (K) strata. This deformation is out-of-sequence, such that the Mesozoic rocks were broadly folded first and then crosscut by more recent thrusting that emplaced the Ordovician rocks over this fold. Photo was taken at Q1 in Figure 1; river width of ~200 m provides approximate scale. White box shows approximate location of view in B. (B) View of north-verging hanging-wall anticline in Ordovician thrust shown in panel A. River for scale is ~100 m wide here. (C) West-dipping normal fault with syntectonic Cretaceous (K) basin-fill deposits. Fault kinematics are dip-slip normal based on observed fault striations and steps within the fault zone. There is no evidence for reactivation of this structure in Cenozoic. Photo was taken near Q1 in Figure 1. (D) Steeply dipping Miocene sediments north of Wulan, which were deposited as foreland basin sediments and then subsequently strongly deformed. (E) View of the south-directed Wulanshan thrust system, which places Proterozoic (Pt) metasedimentary rocks over gently north-dipping Cenozoic (Cz) sediments. This thrust system is the southern boundary of the Qilian Shan–Nan Shan thrust belt, and it connect to the east, along strike, with the Qinghai Nan Shan (e.g., Craddock et al., 2014).

of the southern range front, there are isolated Oligocene–Miocene basin deposits (Qinghai BGMR, 1991) that are steeply tilted today (~80°NE; Fig. 8D). This suggests that following an episode of Oligocene–Miocene exhumation and basin deposition, significant syn- and post-Miocene deformation affected the interior of the Wulanshan.

DISCUSSION

Using a combination of new field observation and existing published data sets, we discuss the tectonic evolution of northern Tibet, from Qaidam Basin in the south to the Hexi Corridor in the north (Fig. 1). Ultimately, the Cenozoic development of this region bears on orogenic plateau formation mechanisms and processes of continental tectonics and plate convergence.

Integrated Shortening Across the Qilian Shan

We integrated available shortening rates across the Qilian Shan thrust belt to see how they match both present-day geodetic convergence rates and our modeled time-dependent shortening rates (Fig. 4). The purpose of this exercise is (1) to demonstrate whether available geologic observations support protracted deformation at a progressively decelerating rate (i.e., ~16 mm/yr to ~6 mm/yr; Fig. 4A) in northern Tibet since the Eocene, and (2) to test our shortening-rate model over the last ~10 m.y. to identify whether it may be valid in the Miocene and older time. We focused on geologic shortening rates (greater than million-year rates) rather than Quaternary rates, which may reflect local spatial or temporal variations of strain during the interseismic loading cycle. Our stain-rate–derived shortening rate curve predicts present-day shortening rates of ~6 mm/yr, which match geodetic convergence rates of 5–7 mm/yr (Fig. 4A; Zhang et al., 2004; Gan et al., 2007). We first tested whether more recent geologic shortening rates (ca. 10–0 Ma) across the Qilian Shan–Nan Shan thrust belt sum to 5–7 mm/yr. There have been recent shortening rate estimates across the North Qilian Shan thrust belt of 3.3 ± 0.6 mm/yr (Zuza et al., 2016a; see also similar but slightly lower estimate by Champagnac et al., 2010) and across the integrated Gonghe Nan Shan and Qinghai Nan Shan of ~0.9 mm/yr (Craddock et al., 2014), which is comparable to the probable ~1 mm/yr shortening rate estimated in this study across the Wulanshan (Fig. 9D). Presently, there are no well-resolved shortening rates estimated across the central Qilian Shan. Based on cross-section restorations across an ~120 km traverse, Zuza et al. (2018) provided some preliminary bounds, although the timing of deformation initiation is uncertain: Rate estimates range from ~1.2 mm/yr assuming ca. 50 Ma deformation initiation to ~4.1 mm/yr assuming ca. 15 Ma initiation. Although speculative, here we assume that the decrease in shortening rate across this central segment follows the same exponential decay as Equation (3) (Fig. 4)—which mirrors the decay in overall plate-convergence velocities (Molnar and Stock, 2009; Copley et al., 2010)—and thus the local shortening rate across the central Qilian Shan decreased from ~5.3 mm/yr at ca. 40 Ma to ~2.9 mm/yr at ca. 10 Ma to ~2.3 mm/yr today. Summing these average rates across the entire width of the Qilian Shan over the last ~10 m.y. yields geologic shortening rates of 6.2–7.4 mm/yr (Fig. 9D), which broadly agree with geodetic convergence and predicted thrust-belt–scale shortening rates (Fig. 4).

Next, we investigated whether available geologic observations suggest an exponential decrease in shortening rate across the thrust system through time, from ~16 mm/yr at ca. 40 Ma to ~10 mm/yr at ca. 10 Ma (Fig. 4). Importantly, this scenario suggests and predicts that more than half of the total Cenozoic shortening strain across the Qilian Shan occurred by the early Miocene. Eocene cooling ages across the central Qilian Shan (Qi et al., 2016; Jian et al., 2018; Du et al., 2018; Li et al., 2019) suggest local exhumation distributed across the region at this time. The Cenozoic Lulehe Formation of northern Qaidam Basin was sourced from the southern Qilian Shan and records the first clastic sedimentation derived from deformation-related uplift. It is traditionally assigned an early Eocene age (Yin et al., 2008b; Yu et al., 2017; Ji et al., 2017; Du et al., 2018; Jian et al., 2018), although Wang et al. (2017) recently suggested a ca. 25.5 Ma age for basal Lulehe strata. We acknowledge that the Lulehe Formation age is debated, but based on early Cenozoic cooling ages observed from across the Qilian Shan, we prefer an Eocene age for the Lulehe Formation. Paleosols sampled from the Lulehe Formation yield $\delta^{18}O$ values that suggest cooling and >1 km uplift of the northern Qaidam Basin since Lulehe deposition (Song et al., 2018). However, these isotopic data should be interpreted with some caution because the Lulehe samples were probably buried deep enough to be significantly heated, and thus potential alteration is a concern (e.g., Jesmok et al., 2018; Song et al., 2018).

Constraints on the magnitude of this early Cenozoic, probable Eocene, shortening are limited. There are two pieces of indirect field evidence that suggest that shortening strain was greater prior to ca. 10 Ma. First, integrating the above deduced ~6 mm/yr over the last ~10 m.y. yields 60 km of shortening across the Qilian Shan thrust belt, which leaves at least ~240 km of remaining shortening (e.g., Meyer et al., 1998; Zuza et al., 2016a, 2018) to have accumulated prior to ca. 10 Ma, at a bulk average shortening rate of ~8 mm/yr from 40 Ma to 10 Ma (Fig. 9D). This is a minimum rate, given that methods of cross-section restorations are minimum estimates (e.g., Judge and Allmendinger, 2011). This is higher than the 10–0 Ma rate, and, depending on the severity of shortening underestimation, the shortening rate could be higher (e.g., >400 km total shortening yields an average rate of >11 mm/yr).

In addition, field observations from the central Qilian Shan suggest that middle Miocene and younger contractional deformation primarily occurred along south-directed thrust faults (Reith, 2013; Zuza et al., 2018). These faults crosscut north-directed thrusts that are presently undated and appear to comprise at least ~60% of the stain across the mapped traverse (Zuza et al., 2018), which equates to ~1.5 mm/yr shortening from 40 Ma to 10 Ma. Reconnaissance thermochronology (Zuza et al., 2016b, 2017b) suggested local exhumation at ca. 50 Ma. Elsewhere across the Qilian Shan, major thrust faults are crosscut by Miocene and younger structures, which obscure the earlier phases of deformation (Zhang et al., 2017). For example, Qi et al. (2016) reported Eocene to middle Miocene exhumation of the central Qilian Shan (~38°02′N, ~99°14′E) as interpreted from AFT track-length modeling. The folds and thrusts in their cross section (Qi et al., 2016, their fig. 2) are consistent with approximately ~30% shortening strain, which, applied over the South Qilian range (i.e., just northwest of Qinghai Lake), would correspond to a rate of ~1.3 mm/yr during this time period (Fig. 9D). Additional pre–middle-Miocene shortening to the south across the Wulanshan/Qinghai Nan Shan is entirely unconstrained. However, given that Wulan Basin sedimentation spanned 22–9 Ma and Wulanshan exhumation initiated at ca. 20 Ma (Lu et al., 2012), and our ~1 mm/yr rate for shortening across the integrated Wulanshan–Qinghai Nan Shan was from ca. 10 Ma to present (Craddock et al., 2014), appreciable shortening and exhumation must have occurred prior to ca. 10 Ma to provide detritus for Wulan Basin. We tentatively suggest at least ~1 mm/yr of shortening occurred across the Wulanshan from ca. 20 Ma to ca. 10 Ma (Fig. 9D), although this is speculative. Finally, approximately ~0.5 mm/yr was estimated across the North Qilian Shan (Zuza et al., 2016a) prior to ca. 10 Ma (Fig. 9D). These observations are consistent with the Qilian Shan having a shortening rate of at least 4–5 mm/yr prior to the middle Miocene (Fig. 9D). This corresponds to 120–150 km shortening from ca. 40 Ma to ca. 10 Ma, roughly half of the ~240 km shortening that has been observed (Zuza et al., 2018), which implies that this rate tabulation

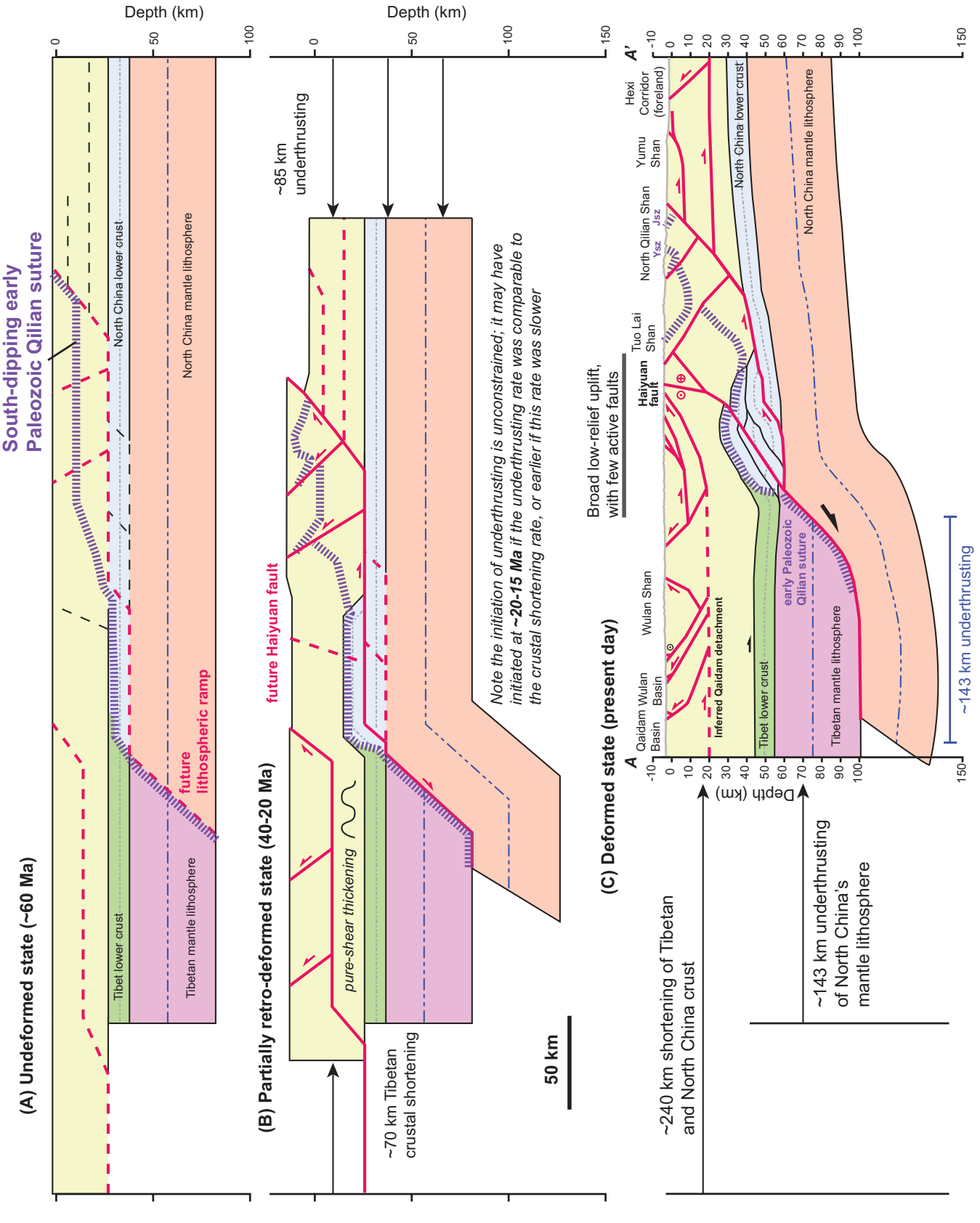

Figure 9. (*Conitinued on following page.*)

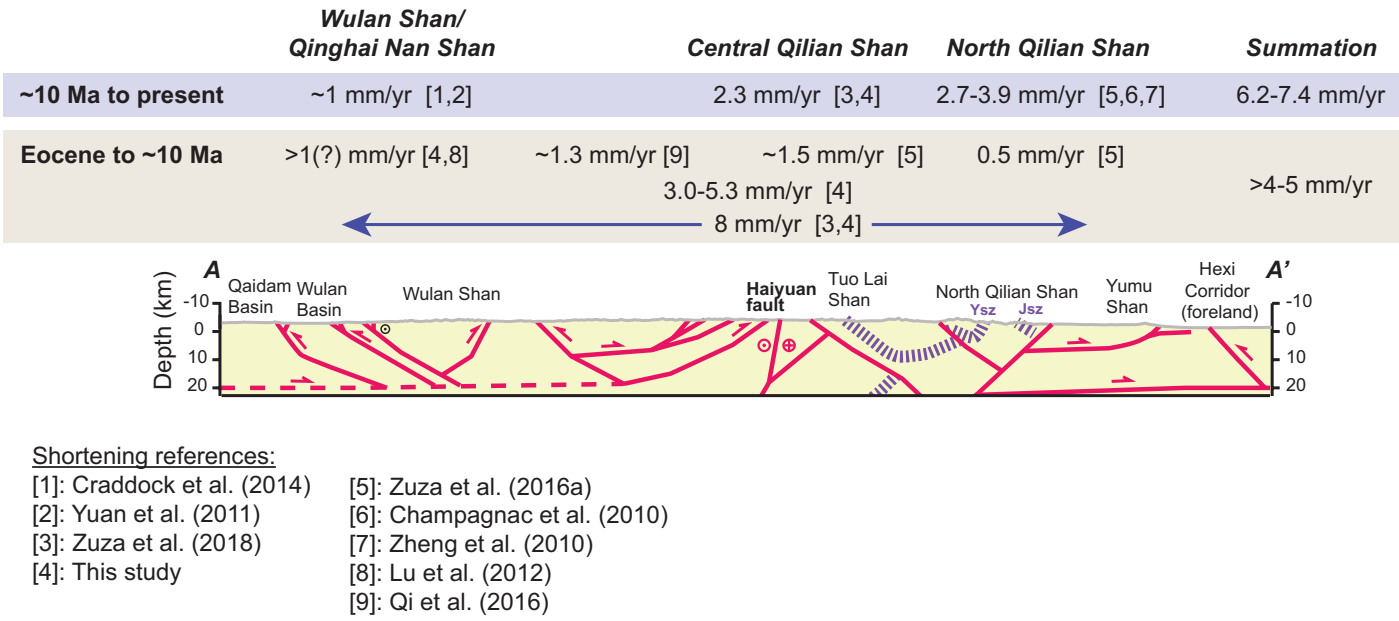

Figure 9 (*continued*). Schematic lithosphere-scale cross section across the Qilian Shan–Nan Shan thrust belt and the northern margin of the Tibetan Plateau, showing our inferred kinematic evolution of this region. Profile A-A′ is shown in Figure 1B. (A) Undeformed state cross section showing inferred configuration of the crust and mantle lithosphere. Section has an initial undeformed width of ~600 km based on existing minimum estimates for crustal shortening across the Qilian Shan thrust belt (Zuza et al., 2016a, 2018). Note the early Paleozoic Qilian suture, which separates North China and Tibetan lithosphere. (B) Early deformation, starting in the Eocene shortly after initial India-Asia collision, reactivates the early Paleozoic Qilian suture. North China mantle lithosphere is underthrust beneath the Tibetan Plateau (e.g., Ye et al., 2015). Crustal faults are shown schematically, and it is envisioned that it thickens via pure shear. Shortening here is drafted conservatively, but this phase of deformation accommodated >155 km of shortening from 40 Ma to 20 Ma. At least ~85 km of underthrusting may have occurred at this time, and the lower crust near the underthrust interface started duplexing and accreting to the base of the Tibetan crust. (C) From the Miocene to preset, underthrusting continued along the early Paleozoic subduction channel, the lower crust thickened via duplexing of North China's lower crust near the mantle-lithosphere ramp structure, and the Tibetan and North China crust was progressively shortened. This schematic cross section shows at least ~240 km of crustal shortening. Two early Paleozoic suture zone localities are also shown: Yushigou (Ysz) and Jiugequan (Jsz). (D) Cropped section from C showing shortening rate estimates across the Qilian Shan.

is missing deformation. Whether the residual ~10 mm/yr of shortening predicted by our shortening-rate model occurred across the Qilian Shan remains unclear and should be the basis for future field studies.

Role of Southward Underthrusting

How the convergence between the India and Asia lithosphere is accommodated in northern Tibet depends on whether or not the upper mantle and crust are coupled (e.g., Burchfiel et al., 1989; Willett and Beaumont, 1994; Gao et al., 1999). Field observations show that the Tibetan crust between the Kunlun fault and the Hexi Corridor (Fig. 1) has deformed by ~30% to 50% shortening strain, but the impact of continental plate convergence on the mantle lithosphere of Tibet or Eurasia is less well constrained. Models of vertically uniformly distributed shortening (e.g., Dewey and Bird, 1970; Dewey and Burke, 1973; England and Houseman, 1986) suggest thickening of the mantle lithosphere; for example, 50% shortening strain should double the thickness of the mantle lithosphere, assuming pure-shear thickening. Although central Tibet may have thickened mantle lithosphere, northern Tibet does not appear to have been extensively thickened (e.g., Priestley and McKenzie, 2013).

Alternatively, as postulated by some geophysical studies, including deep-seismic reflection profiling and more recent receiver function analyses, the mantle lithosphere of the North China craton may be underthrusting the northern Tibetan Plateau (e.g., Willett and Beaumont, 1994; Gao et al., 1999; Feng et al., 2014; Ye et al., 2015). That is, the crust and upper mantle along the northern boundary of the Tibetan Plateau are decoupled. More recent anisotropy and seismic velocity studies also corroborate underthrusting (e.g., Huang et al., 2017; Ding et al., 2017), although this hypothesis remains debated (Wei et al., 2017). These models suggest that the southern edge of the North China craton's mantle lithosphere is underthrusting from the northern plateau margin to a position underneath northern Qaidam Basin (Fig. 1A). The southward motion of North China's mantle lithosphere beneath the Tibetan crust and mantle lithosphere would presumably be associated with equivalent-magnitude shortening in the middle-to-upper crust as it resisted subduction (i.e., crustal accretion; see Himalayan examples: Capitanio et al., 2010; Webb, 2013; Gao et al., 2016). We envision that this process would result in focused deformation along the underthrusting interface, such that higher strain magnitudes should exist along the boundary between North China and Tibet. Indeed, relatively large-magnitude upper-crustal shortening (i.e., >50 km shortening or >50% shortening strain) has been documented along the interface between the Tibetan Plateau and North China in the North Qilian Shan (Zuza et al., 2016a). Roughly two thirds of total present-day convergence across the thrust belt is accommodated along this northern frontal thrust zone.

There are two caveats to the above interpretation:

(1) Upper-crustal shortening may represent a combination of underthrusting accommodation and vertically coherent shortening strain of the Tibetan lithosphere. That is, the total convergence magnitude should equal

the sum of underthrust magnitude and internally distributed vertically uniform lithospheric shortening. Thus, the magnitude of underthrusting is less than or equal to total lithospheric shortening.

(2) The initiation of underthrusting and crustal shortening may have occurred at different times. The timing of underthrusting cannot be constrained from geophysical methods, and it may have occurred anytime during the Cenozoic or potentially earlier (Allen et al., 2017). Earlier underthrusting initiation implies a slower bulk rate of underthrusting, whereas more recent initiation requires faster rates.

Duplex Development Beneath the Qilian Shan

As stated above, the underthrusting process predicts that the magnitude of underthrusting of the mantle lithosphere should be equal to or less than observed crustal shortening strain as North China's crust resists subduction beneath the Tibetan mantle lithosphere. Shortening strain may occur via crustal-scale faults that accommodate vertically coherent horizontal shortening from the upper to lower crust. Alternatively, if the lower and middle-upper crust is decoupled (e.g., Burchfiel et al., 1989; Gao et al., 1999), different styles of deformation are expected between crustal layers, which may include lower-crustal duplex development or channelized flow of low-viscosity layers in response to horizontal pressure gradients (e.g., Clark and Royden, 2000; Gao et al., 2016). We prefer a model with several detachment horizons and duplexes for the following reasons:

(1) Several detachment horizons in the lower and middle crust have been imaged seismically (Gao et al., 1999), which may have favored decoupled deformation at different crustal levels (Burchfiel et al., 1989). In addition, the preexisting weaknesses associated with the early Paleozoic Qilian orogen (Allen et al., 2017; Zuza et al., 2018) may have facilitated local duplexing in horizons of concentrated subduction-mélange material, which would involve friction-reducing clays, hydrated phyllosilicates, and relatively low-viscosity sediments (e.g., Collettini et al., 2009; Behr and Becker, 2018).

(2) The topography and geomorphology in the central Qilian Shan around the Haiyuan fault, as interpreted by Zhang et al. (2017), show uplifted relict erosional surfaces suggesting crustal-scale upwarping (Craddock et al., 2014; Zhang et al., 2017). Thrust faults, earthquakes, and high-relief landscapes are concentrated on the margins of this broad upwarp (Craddock et al., 2014; Allen et al., 2017).

(3) There is a local crustal thickness maximum in the location of our inferred duplex (Fig. 1C; Yue et al., 2012; Tian et al., 2014; Xu et al., 2018). Although there is a smooth decrease in crustal thickness to the east along strike of the Qilian Shan, the north-south variations are more erratic. The crust in the central Qilian Shan is ~10 km thicker than to the north and south (Tian et al., 2014), and as noted previously, this location has fewer surface-breaching thrust faults, particularly active faults, than other areas of the Qilian Shan (e.g., Allen et al., 2017). The crustal thickness of Qaidam Basin is ~10 km thinner than the Qilian Shan, despite the magnitude of crustal shortening being comparable (e.g., Yin et al., 2008a, 2008b; Zuza et al., 2016a, 2018). Therefore, it appears that crustal thickening here locally requires some other source, such as duplexing or channelized flow of the lower crust.

(4) Recent receiver function analyses by Xu et al. (2018) showed a complicated pattern of thickened crust beneath the Hexi Corridor, varying from ~45 km to 55 km thick, which does not appear to match surface fold or fault structures. Middle-crust detachments and passive thickening via duplexing and lower-crustal accretion could explain these local variations in crustal thickness.

(5) Lastly, this region is the location of the lithospheric ramp that accommodates the southward underthrusting of the Asian mantle lithosphere (Feng et al., 2014; Ye et al., 2015; this study). This structure could focus our inferred duplex development as the lower crust resists subducting deeper and is underplated and/or accreted to the Tibetan crust.

Although the above evidence suggests a duplex structure, we recognize that alternative scenarios are possible. For example, there could have been passive thickening of the crust around the Haiyuan fault latitude via lower-crustal flow; the same regions in which we envision duplexing could have thickened via channel flow processes. However, we prefer the duplex model on the basis of seismic reflection imaging, which does not reveal subhorizontal shear zones as predicted by channel flow models, but rather warped and folded reflectors suggesting folding and faulting in the middle and lower crust, such as folded duplex thrust sheets (Wang et al., 2011; Gao et al., 2013; Guo et al., 2016). In addition, horizontal crustal shortening values observed across northern Tibet are more than enough to vertically thicken the crust (Gaudemer et al., 1995; Meyer et al., 1998; Yin et al., 2008a, 2008b; Lease et al., 2012; Zuza et al., 2016a, 2018), which means additional crustal thickening due to a lower-crustal channel flow process would be expected to overthicken the crust. Given erosion magnitudes are <5 km, it is hard to imagine how this overthickened crusted could be thinned to observed present-day crustal thickness values.

Integrated Kinematic Model for the Development of the Qilian Shan

Based on our new field observations, existing geophysical data, and the inferences discussed above, we present a new kinematic model for the evolution of the northern Tibetan Plateau that is summarized in the cross-section model in Figure 9. Prior to the Cenozoic, the Tibetan and North China lithospheres were separated by the early Paleozoic Qilian suture, and the crust was ~35 km thick (Fig. 9A). North Tibet started deforming quickly after initial India-Asia collision at ca. 58 Ma (e.g., DeCelles et al., 2014; Hu et al., 2015, 2016), broadly exploiting the mechanically weak Qilian suture zone as a lithosphere-scale thrust ramp (Fig. 9B). Tibetan crust deformed and thickened around the North Qaidam and Wulanshan thrust systems (Fig. 9B; and related Olongbulak thrust; Yu et al., 2017). We envision that underthrusting of North China's mantle lithosphere beneath Tibet initiated sometime during this time interval, although the exact timing remains unresolved. If underthrusting was delayed, partial pure-shear thickening of the mantle lithosphere must have occurred to accommodate convergence (e.g., Priestley and McKenzie, 2013). Underthrusting occurred along the relict suture zone, and the middle and upper crust above this underthrust ramp deformed to accommodate North China's southward motion (Fig. 9B). Duplexing of the lower crust occurred at the mantle lithosphere ramp and passively thickened the crust around Qinghai Lake and the future Haiyuan fault trace (Fig. 1). From the Eocene to early Miocene, we envision this region accommodated at least ~150 km of Tibet-Asia convergence.

From the Miocene to present, underthrusting and crustal shortening continued along the same lithospheric ramp, and North China's lower crust continued to form duplex structures at this ramp as it resisted being subducted beneath Tibetan mantle lithosphere (Fig. 9C). The Tibetan crust around this duplex was passively thickened, forming a high-elevation and low-relief landscape (Zhang et al., 2017) with minimal active surface-breaching thrust faults (Allen et al., 2017). The Haiyuan left-slip fault, and the relatively minor Riyueshan and Elashan right-slip faults, initiated at around ca. 15–10 Ma near this ramp structure, facilitated by a combination of the preexisting weakness of the early Paleozoic suture zone and overthickening of the crust (Fig. 9C). The highest magnitude of crustal shortening was concentrated along the northern plateau margin, at the interface between the underthrusting North China and overriding Tibetan

lithosphere. Net underthrusting of North China is ~150 km, as suggested by geophysical studies (Fig. 9C; Ye et al., 2015).

What is not shown because of the scale of this cross section and its schematic nature are crosscutting relationships. However, it should be noted that deformation was concentrated in the north Tibetan crust over at least ~40 m.y., with minimal foreland advancement. The prominent exception is the northward-propagating thrusts underlying the Yumu Shan that advanced into the Hexi Corridor, which has occurred only over the last several million years (e.g., Tapponnier et al., 1990; Hu et al., 2017). That said, the North Qilian Shan remained the approximate northern plateau boundary during Cenozoic deformation (Clark, 2012).

Location of Underthrust Ramp

The position of the lithospheric ramp that accommodates southward underthrusting of North China beneath Tibet (Fig. 9) to approximately the latitude of Qaidam Basin (Fig. 1; e.g., Ye et al., 2015) is critical for the location and style of crustal deformation, including our inferred lower-crustal duplexing (Fig. 10). This is because we infer that the lower crust of North China resists subduction beneath the Tibetan Moho and mantle lithosphere. Therefore, the simplest scenario is for both lower- and upper-crustal deformation to concentrate toward the foreland of this large underthrust system (Fig. 10), similar to the Himalaya (e.g., Long et al., 2011; Webb, 2013; Haproff et al., 2018). The position of the lithospheric ramp may be located at one of two end-member locations, assuming net underthrusting of North China's mantle lithosphere to approximately the latitude of northern Qaidam Basin (Fig. 1): either (1) a northern ramp position near the present-day margin of the plateau, or (2) a southern position underneath the Haiyuan fault (Fig. 10). If the ramp is in the south, a similar magnitude of upper- and lower-crustal shortening, S_1, is predicted to the north of this ramp location in the Qilian Shan thrust belt (left panel in Fig. 10). If the ramp is located to the north by the plateau's northern margin, a higher magnitude of mantle-lithosphere underthrusting, and therefore crustal shortening, S_2, is predicted (i.e., $S_2 > S_1$). This upper-crustal shortening should occur north of the ramp location, in the relatively undeformed Hexi Corridor foreland basin (central panel in Fig. 10). We envision one mechanism to reconcile a northern ramp location: wedge tectonics, where southward underthrusting of North China's mantle lithosphere is fed to south-directed faults in the central Qilian Shan (right panel in Fig. 10). This requires a high magnitude of shortening, S_2, which matches a high magnitude of North China underthrusting.

Through these geometric arguments, we can better refine the magnitude of continental underthrusting along the plateau's northern margin. The northern ramp option, located beneath the North Qilian Shan (i.e., the Tibet–North China interface), suggests that upper-crustal shortening that accommodates southward underthrusting should have occurred at this interface and to the north in the Hexi Corridor (Figs. 1 and 10). However, Cretaceous–Cenozoic strata in the Hexi Corridor are essentially undeformed (see seismic profiles in Zuza et al., 2016a), which means that all of the deformation associated with underthrusting is accommodated to the south of the plateau's margin. Instead, we suggest that the mantle-lithosphere ramp is located around the latitude of the Haiyuan fault (Figs. 9 and 10). This position may explain deformational features here, as discussed above, and requires a relatively lower magnitude of total underthrusting of ~150 km. We note that this ramp could be conceivably located beneath the North Qilian Shan and Hexi Corridor if a wedge-tectonic scenario is operating (Fig. 10).

Initiation Mechanism for Strike-Slip Faulting in Northern Tibet

Strike-slip fault initiation in the Qilian Shan occurred around ca. 15–10 Ma, roughly 30 m.y. after shortening initiated there (Yuan et al., 2013; Duvall et al., 2013; Li et al., 2019). A two-stage development of the Qilian Shan has been proposed, with early thrusting transitioning to mixed-mode thrust-and-strike-slip faulting (Lease et al., 2012; Yuan et al., 2013) in the middle Miocene. However, if the strain rate across the orogen has remained constant (Clark, 2012), this implies a constant stress, and this thrust-to-strike-slip faulting transition may instead have resulted from protracted deformation.

Based on the kinematic model presented in this study, we hypothesize that the initiation of strike-slip faulting may have occurred due to progressive overthickening of the crust, leading to a switch of the intermediate compressive stress orientation from horizontal to vertical (Fig. 11).

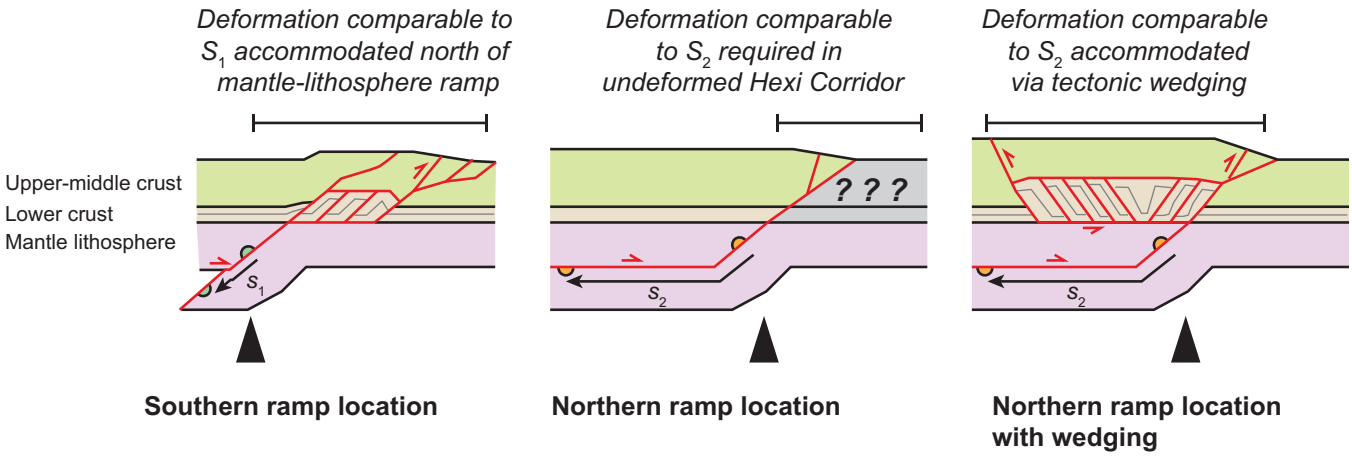

Figure 10. Diagram illustrating how the location of the inferred mantle-lithosphere ramp impacts shortening magnitudes and locations. If the ramp is located near the southern margin of the Qilian Shan–Nan Shan thrust belt, the underthrusting magnitude should be comparable to the magnitude of crustal shortening north of the ramp. If the ramp is located in the north, near the plateau margin, the simple explanation requires shortening, of similar magnitude to the underthrust amount, to have occurred north of the plateau in the Hexi Corridor foreland. An alternative scenario to reconcile the issues with a northern ramp location is if tectonic wedging occurs, such that deformation associated with underthrusting of North China's mantle lithosphere occurs south of the mantle-lithosphere ramp location.

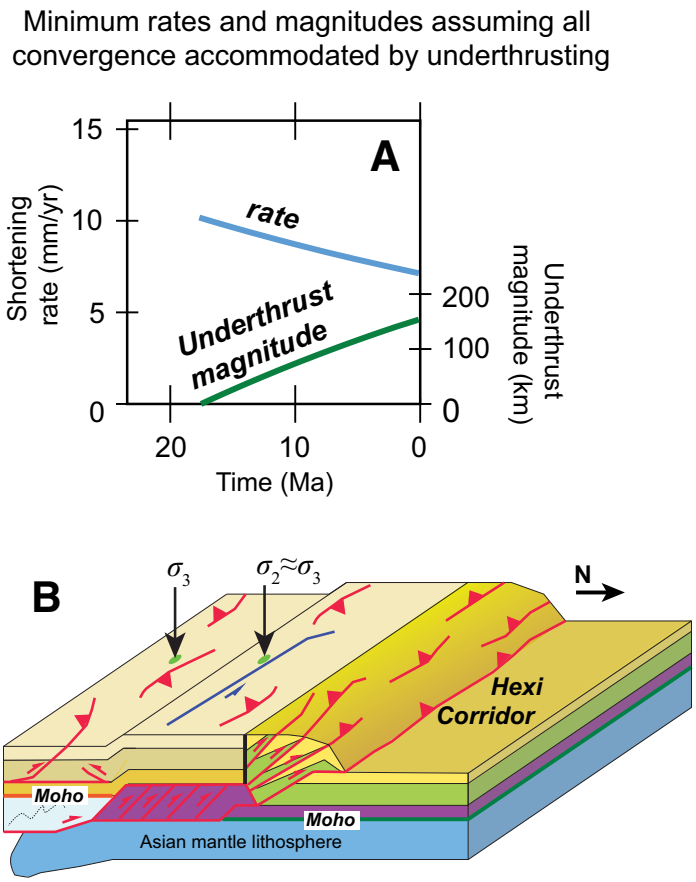

Figure 11. (A) Magnitude of underthrusting in the late Cenozoic predicted by our modeled shortening rates across northern Tibet. This plot was constructed by first assuming a total of ~150 km of underthrusting of North China today, as discussed in the text, and then restoring this underthrusting based on predicted shortening rates across the Qilian Shan. Note that this plot predicts that underthrusting initiated at ca. 20–15 Ma, which is approximately when strike-slip faulting started in northern Tibet (Duvall et al., 2013). (B) Model for how lower-crustal duplexing caused by North China underthrusting beneath Tibet can initiate strike-slip faulting in northern Tibet. As North China underthrusts the Tibetan Plateau, its lower crust is accreted to the base of the Tibetan lower crust via duplexing. This thickens the Tibetan crust, which rotates the intermediate compressive stress orientation (σ_2) from horizontal to vertical, driving a transition from thrust-dominated (i.e., vertical σ_3) to mixed-mode deformation involving thrust and strike-slip faulting.

Specifically, this may have been driven by lower-crust duplexing near the main lithospheric ramp for southward underthrusting, as discussed above. This process would have passively thickened the crust via duplex underplating, causing a rotation of the intermediate compressive stress orientation to vertical.

Our model implies ~150 km underthrusting of North China beneath Tibet, and if we restore this underthrusting at the time-varying rates modeled in the section on "Kinematics of the Tibetan Plateau's Northern Margin" (Fig. 4), we find that underthrusting initiated at ca. 20–15 Ma. This is a maximum rate, as it assumes that all of convergence was accommodated via underthrusting; it instead may have been partitioned between underthrusting and distributed vertically coherent lithospheric shortening. However, it is interesting to note that the estimated 20–15 Ma initiation of underthrusting coincides with the estimated timing when strike-slip faulting became a dominate deformation mechanism in northern Tibet. We speculate that the process of underthrusting may control the style of deformation in the upper crust, as has been postulated elsewhere in Tibet (e.g., Molnar et al., 1993; Styron et al., 2015). Alternatively, initiation of both underthrusting and strike-slip faulting may be responses to protracted crustal thickening.

Implications for the Evolution of the Himalayan-Tibetan Orogen

A cross section drawn across the Himalayan-Tibetan orogen and Tibetan Plateau, parallel to north-northeast–trending India-Asia convergence, involves the Himalaya to the south and the Qilian Shan to the north (Fig. 1). These two thrust belts balance body forces associated with the high gravitational potential energy (GPE) of the ~70-km-thick Tibetan Plateau (England and Houseman, 1989; Molnar et al., 1993; England and Molnar, 1997). Therefore, the evolution of this entire system and the growth of the plateau depend on the structural framework of these thrust belts. The overall architectures of the Himalaya and Qilian Shan are comparable: Both involve continental underthrusting, crustal-scale imbrication, and duplexing along the convergence-perpendicular margins of the Himalayan-Tibetan orogen (Argand, 1924; Powell and Conaghan, 1973; DeCelles et al., 2002; Gao et al., 1999, 2013, 2016; Zuza et al., 2016a, 2018; this study). Interestingly, these similarities between the orogen-scale architectures persist despite vastly different climatic and plate-velocity boundary conditions (Table 1; Figs. 12 and 13), as discussed below. This begs the question: What factors control the style of orogenesis (e.g., Mouthereau et al., 2013)? For example, there is a long-standing debate whether climate and erosion affect the style and magnitude of continental deformation (e.g., Avouac and Burov, 1996; Beaumont et al., 2001; Whipple and Meade, 2004; McQuarrie et al., 2008).

TABLE 1. COMPARISON OF HIMALAYA AND QILIAN SHAN–NAN SHAN THRUST BELTS

Feature	Himalaya	Qilian Shan	Difference	Refs.
Contemporary convergence rate	25–20 mm/yr	7–5 mm/yr	4 ± 1×	1–2
Minimum shortening magnitude	1600–750 km	350–250 km	4 ± 2×	3–6
Underthrust magnitude	1000–750 km	~150 km	5–6×	7–11
MAP	4000–1000 mm/yr	350–100 mm/yr	**22 ± 19×**	12–13
Cooling ages* (and exhumation magnitude)	Cz < 10–15 Ma (>20 km)	Pz-Mz >ca. 50–150 Ma (<5 km)	**~10 ± 5×** (4×)	14–19

Note: Differences greater than an order of magnitude are shown in bold. MAP—mean annual precipitation, Cz—Cenozoic; Mz—Mesozoic; Pz—Paleozoic. References: 1—Zhang et al. (2004), 2—Gan et al. (2007), 3—DeCelles et al. (2002), 4—Webb et al. (2011), 5—Long et al. (2011), 6—Zuza et al. (2016b), 7—Schulte-Pelkum et al. (2005), 8—Nábělek et al. (2009), 9—Styron et al. (2015), 10—Ye et al. (2015), 11—this study, 12—Hijmans et al. (2005), 13—Bookhagen (2014), 14—George et al. (2001), 15—Jolivet et al. (2001), 16—Zheng et al. (2010), 17—Thiede and Ehlers (2013), 18—McQuarrie and Ehlers (2015), and 19—Qi et al. (2016).

*Thermochronometric data from apatite fission track, zircon (U-Th)/He, or higher-temperature systems; lower-temperature systems, including apatite (U-Th)/He, are excluded because they are significantly affected by topographic relief and may vary with elevation.

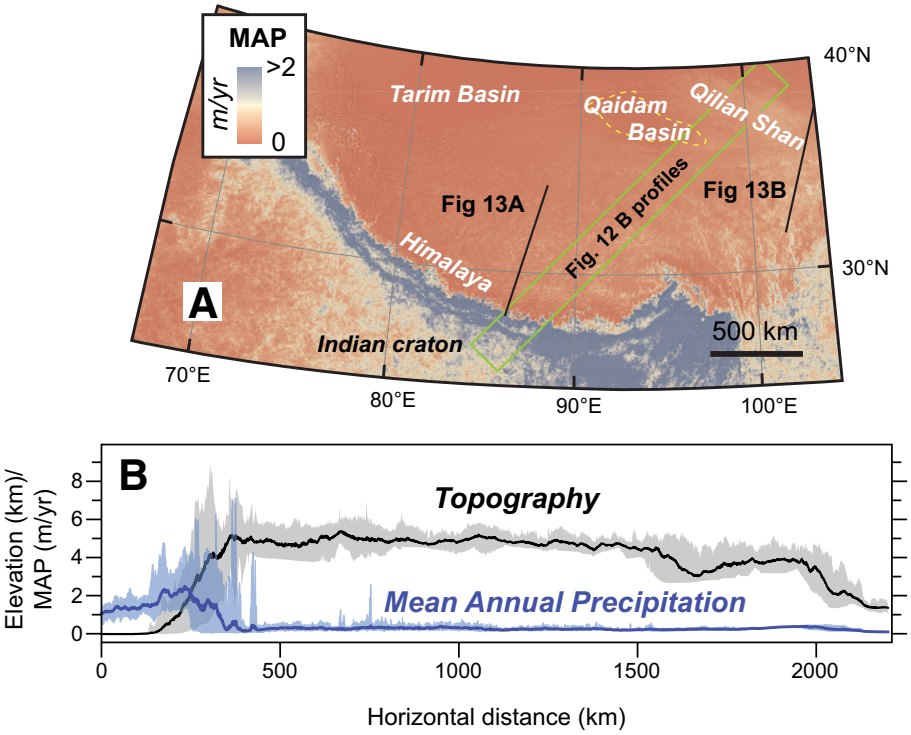

Figure 12. (A) Mean annual precipitation (MAP) for the Tibetan Plateau. Data are primarily from Bookhagen (2014), supplemented with data from Hijmans et al. (2005), available at http://www.worldclim.org/. Green box shows 200-km-wide swath profile for precipitation and topography plots in part B, and black lines show geophysical surveys in Figure 13. (B) MAP (blue line) and topography (black line) along the 200-km-wide swath in Figure 13A. Thick solid line represents mean value, and shaded region encompasses the maximum and minimum values in the swath profile.

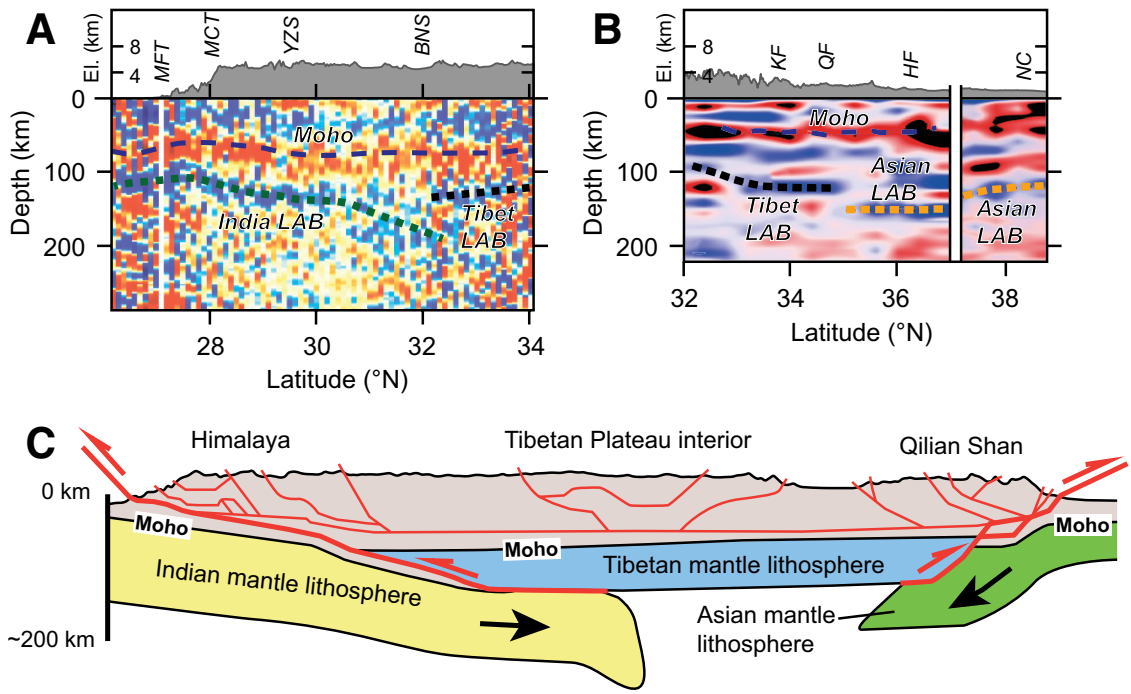

Figure 13. Geophysical and interpreted schematic cross sections across the Himalayan-Tibetan orogen, showing S-receiver function profiles across (A) the Himalaya–southern Tibet (Zhao et al., 2010) and (B) northern Tibet (Ye et al., 2015). Locations for A and B are shown in Figure 12. (C) Schematic cross section of the Himalayan-Tibetan orogen and minimum magnitudes of continental underthrusting along the northern and southern plateau margins were derived from DeCelles et al. (2002), Nábělek et al. (2009), Zhao et al. (2010), Styron et al. (2015), Ye et al. (2015), and Zuza et al. (2016a). Abbreviations: MFT—Main Frontal thrust; MCT—Main Central thrust; BNS—Bangong-Nujiang suture; KF—Kunlun fault; LAB—Lithosphere-asthenosphere boundary; QF—Qinling fault; HF—Haiyuan fault; NC—North China craton; YZS—Yarlung-Zangbo suture.

Overall present-day convergence rates across the Himalaya are four times greater than that of the Qilian Shan, which correlates with four times greater magnitudes of crustal shortening and continental underthrusting (Table 1; Fig. 13; Powell and Conaghan, 1973; DeCelles et al., 2002, 2011; Schulte-Pelkum et al., 2005; Nábělek et al., 2009; Yin et al., 2010; Zhao et al., 2010; Long et al., 2011; Webb et al., 2011; Styron et al., 2015; Zuza et al., 2016a, 2018). Given the exponential decrease in India-Asia convergence rates (Molnar and Stock, 2009; Copley et al., 2010), these rates and shortening magnitudes have also probably decreased proportionally throughout the Cenozoic. Mean annual precipitation across the Tibetan Plateau decreases from meters per year across the Himalaya to <35 cm/yr across the Qilian Shan (Hijmans et al., 2005; Bookhagen et al., 2005; Bookhagen and Burbank, 2006; Bookhagen, 2014; see also Fig. 12). Isotopic and paleontological data suggest that northern Tibet has been similarly dry since the start of the Oligocene (e.g., Wang et al., 2003; Dupont-Nivet et al., 2007). The Eocene climate in northern Tibet is less well constrained, including whether it was a warmer and wetter time period (e.g., Dupont-Nivet et al., 2008; Jesmok et al., 2018). The across-strike Tibetan Plateau precipitation variations correlate with denudation and exhumation. AFT and higher-temperature thermochronometers from samples across the Himalaya yield Cenozoic ages of <15–10 Ma, corresponding to exhumation magnitudes of >20 km (e.g., Thiede and Ehlers, 2013; McQuarrie and Ehlers, 2015). Conversely, similar system cooling ages from the Qilian Shan are generally Mesozoic or older, and exhumation is estimated to be <5 km (George et al., 2001; Jolivet et al., 2001; Zheng et al., 2010; Qi et al., 2016; see also Table 1).

In summary, these observations suggest that while the absolute magnitude of crustal shortening and underthrusting is controlled primarily by total convergence across each thrust system, the orogenic architecture of the northern and southern margins of the Himalayan-Tibetan orogen (Fig. 13) is not strongly affected by climate or plate-velocity forcing mechanisms. Despite different convergence rates and climate-related erosion/exhumation rates, the two thrust belts involve similar deformational processes, including underthrusting and duplexing. Instead, the overall thrust-belt structure may be controlled by the age, temperature, and related strength of the deforming lithosphere (e.g., Kong et al., 1997; Mouthereau et al., 2013). A compilation of global orogens by Mouthereau et al. (2013) revealed continental underthrusting is predicted for orogens with a relatively old, cold, and strong foreland, whereas thrust belts in young warm lithosphere are expected to involve vertically coherent pure-shear deformation. The Tibetan crust, with a relatively low elastic thickness (T_e; e.g., T_e < ~20 km; Braitenberg et al., 2003), is bounded to the north and south by the Archean–Proterozoic North China and Indian cratons, respectively, which predicts underthrusting-style deformation around the Tibetan Plateau margins (Mouthereau et al., 2013). Furthermore, deformation focused along preexisting weaknesses in northern Tibet related to the early Paleozoic Qilian orogen, such that this south-dipping subduction channel was favorably oriented to serve as a ramp structure to initiate and facilitate south-directed continental underthrusting. Ultimately, the orogenic structural style in the Himalayan-Tibetan orogen may be attributed to strength heterogeneities in predeformational crust (e.g., Kong et al., 1997; Chen and Gerya, 2016; Mouthereau et al., 2013).

That said, the kinematic development of the Qilian Shan–Nan Shan thrust belt is distinct from the Himalaya for two reasons. First, the Qilian Shan is relatively wide (~350 km), especially given its lower convergence rate and magnitude, compared to the Himalaya (~250 km). Second, shortening across the Himalaya is presently concentrated almost entirely along the Main Frontal thrust (Lavé and Avouac, 2000; Burgess et al., 2012), whereas the Qilian Shan has active shortening distributed across the thrust belt (Meyer et al., 1998; Allen et al., 2017; this study). The lower precipitation (Fig. 12) and limited focused erosion in the Qilian Shan compared to the Himalaya may facilitate these differences (e.g., Avouac and Burov, 1996; Willett, 1999; Beaumont et al., 2001; Whipple and Meade, 2004; McQuarrie et al., 2008). Wide distributed deformation in northern Tibet may reflect a mechanically weak basal detachment beneath the Qilian Shan, which also predicts the observed low-angle taper and substantial back thrusting (e.g., Burg et al., 1994; Malavieille, 2010). This weak detachment horizon would be either a subduction-mélange channel of the early Paleozoic Qilian orogen (Song et al., 2013; Zuza et al., 2018) or weak and flowing low-viscosity lower crust (Bird, 1991; Clark and Royden, 2000). The early Paleozoic Qilian suture zone may serve as this preexisting weakness with friction-reducing clays and hydrated phyllosilicates (e.g., Collettini et al., 2009; Behr and Becker, 2018). This south-dipping paleo–subduction system (Zuza et al., 2018) was thus favorably oriented to serve as a ramp structure to initiate and facilitate south-directed continental underthrusting. On the other hand, evidence for lower-crustal flow in this region of the plateau is inconclusive (Lease et al., 2012; Zuza et al., 2016a).

The Qilian Shan has persisted as the northern boundary of the Himalayan-Tibetan orogen and Tibetan Plateau since shortly after India-Asia collision. Given that deformation initiated here shortly after collision (Dupont-Nivet et al., 2004; Clark et al., 2010; Yin et al., 2008a, 2008b; Craddock et al., 2011), a typical foreland-propagating thrust belt would be expected to migrate northward through progressive footwall/foreland accretion and/or overthrusting, thus moving the northern orogen boundary northward. However, the Qilian Shan thrust belt did not propagate northward during the Cenozoic, which is an inference that is supported by the undeformed nature of the Hexi Corridor, with ~5–10 km of parallel Cenozoic–Cretaceous sediments (e.g., Li and Yang, 1998; Zhuang et al., 2011; Zuza et al., 2016a). Over the last several million years, several thrust splays have advanced into the basin, as indicated by thermochronology studies along basin-bounding thrust panels (Zheng et al., 2010, 2017). Our observations of the exposed hanging-wall flat in the Hexi Corridor (Fig. 6) corroborates some northward growth of the plateau, which may be related to local plateau expansion due to critical overthickening of the central Qilian Shan to the south. A stationary northern boundary suggests that the Qilian Shan–Nan Shan thrust belt has persisted as an out-of-sequence thrust system to preserve North China as a relatively undeformed block.

CONCLUSIONS

In this study, we presented field observations from a geological traverse across the Qilian Shan thrust belt in northern Tibet that demonstrate that protracted and overprinting Cenozoic contractional deformation has affected this region since the Eocene. We also developed a strain-rate–based shortening model to compare against field-based shortening estimates, which suggests an overall decrease in shortening rate in northern Tibet from ~16 mm/yr to ~6 mm/yr that correlates with the decreasing India-Asia convergence rates through the Cenozoic. This requires that most of the shortening strain in northern Tibet occurred prior to the middle Miocene. Available geologic shortening rate observations and crosscutting relationships discussed herein are consistent with this model, although more constraints of pre-middle Miocene deformation are required.

By integrating new field observations with published shortening studies, thermochronology, and geophysical surveys, we developed a lithospheric-scale tectonic model for the development of the northern margin of the Tibetan Plateau. Key factors in this model are progressive convergence between Tibet and Asia since the Eocene, ~150 km of southward underthrusting of North China's mantle lithosphere along an early Paleozoic subduction mélange complex, and duplexing of North China's lower crust

and related passive uplift of the central Qilian Shan. Duplexing may have occurred along the underthrusting ramp as North China crust resisted subducting beneath Tibetan lithosphere, which can explain the high elevation, low relief, relative aseismicity, and thickened crust of the central Qilian Shan. Ultimately, our integrated model for the development of the northern Tibetan Plateau explains available field and geophysical observations. Some aspects of our modeled tectonic history and time-varying shortening evolution are speculative, but these provide an updated framework to be tested via future field, geophysical, and geochemical studies.

The south-dipping early Paleozoic Qilian suture acted as an important preexisting weakness in northern Tibet to focus deformation, and its position probably assisted in the decoupling of the crust and mantle lithosphere during southward underthrusting. This suture zone thus helped to define the northern extent of the Cenozoic Tibetan Plateau. The Miocene initiation of strike-slip faulting along the Haiyuan and Kunlun faults paralleled pre-Cenozoic suture zones, which further suggests that strength anisotropies are critical in controlling deformation across the Himalayan-Tibetan orogen.

The Cenozoic evolution of northern Tibet is similar to that of the Himalaya; both involving large-scale underthrusting of mantle lithosphere beneath Tibet. These similarities persist despite different climatic and plate-velocity boundary conditions, suggesting that the orogen-scale architecture of these thrust belts bounding the Tibetan Plateau is controlled by neither of these forcing mechanisms. The style and location of deformation around the plateau are instead controlled by local strength anisotropies, such as preexisting weaknesses like pre-Cenozoic sutures, which focus deformation.

ACKNOWLEDGMENTS

This research was supported by the China Geological Survey (DD20160083), the National Science Foundation of China (Project no. 41702232), the fundamental Research Funds for the Central Universities (C. Wu), the Tectonics Program of the National Science Foundation, and startup funds at University of Nevada, Reno. We appreciate thorough reviews by Mike Murphy, Jay Chapman, and Feng Cheng that improved the ideas presented in this manuscript.

REFERENCES CITED

Allen, M.B., Walters, R.J., Song, S., Saville, C., De Paola, N., Ford, J., Hu, Z., and Sun, W., 2017, Partitioning of oblique convergence coupled to the fault locking behavior of fold-and-thrust belts: Evidence from the Qilian Shan, northeastern Tibetan Plateau: Tectonics, v. 36, no. 9, p. 1679–1698, https://doi.org/10.1002/2017TC004476.

Argand, E., 1924, La Tectonique de l'Asie: Proceedings of the 13th International Geological Congress, v. 7, p. 171–372.

Avouac, J.P., and Burov, E.B., 1996, Erosion as a driving mechanism of intracontinental mountain growth: Journal of Geophysical Research, v. 101, p. 17,747–17,769, https://doi.org/10.1029/96JB01344.

Baotian, P., Qingyang, L., Xiaofei, H., Haopeng, G., Zibian, L., Shaofei, J., and Wanming, Y., 2013, Cretaceous and Cenozoic cooling history of the eastern Qilian Shan, north-eastern margin of the Tibetan Plateau: Evidence from apatite fission-track analysis: Terra Nova, v. 25, no. 6, p. 431–438, https://doi.org/10.1111/ter.12052.

Beaumont, C., Jamieson, R.A., Nguyen, M.H., and Lee, B., 2001, Himalayan tectonics explained by extrusion of a low-viscosity crustal channel coupled to focused surface denudation: Nature, v. 414, p. 738–742, https://doi.org/10.1038/414738a.

Behr, W.M., and Becker, T.W., 2018, Sediment control on subduction plate speeds: Earth and Planetary Science Letters, v. 502, p. 166–173, https://doi.org/10.1016/j.epsl.2018.08.057.

Bird, P., 1991, Lateral extrusion of lower crust from under high topography in the isostatic limit: Journal of Geophysical Research, v. 96, p. 10,275–10,286, https://doi.org/10.1029/91JB00370.

Bookhagen, B., 2014, High Resolution Spatiotemporal Distribution of Rainfall Seasonality and Extreme Events Based on a 12-Year TRMM Time Series: http://www.geog.ucsb.edu/~bodo/TRMM/ (accessed December 2016).

Bookhagen, B., and Burbank, D.W., 2006, Topography, relief, and TRMM-derived rainfall variations along the Himalaya: Geophysical Research Letters, v. 33, L08405, https://doi.org/10.1029/2006GL026037.

Bookhagen, B., Thiede, R.C., and Strecker, M.R., 2005, Late Quaternary intensified monsoon phases control landscape evolution in the northwest Himalaya: Geology, v. 33, p. 149–152, https://doi.org/10.1130/G20982.1.

Bovet, P.M., Ritts, B.D., Gehrels, G., Abbink, A.O., Darby, B., and Hourigan, J., 2009, Evidence of Miocene crustal shortening in the north Qilian Shan from Cenozoic stratigraphy of the western Hexi Corridor, Gansu Province, China: American Journal of Science, v. 309, p. 290–329, https://doi.org/10.2475/00.4009.02.

Braitenberg, C., Wang, Y., Fang, J., and Hsu, H.T., 2003, Spatial variations of flexure parameters over the Tibet-Quinghai plateau: Earth and Planetary Science Letters, v. 205, p. 211–224, https://doi.org/10.1016/S0012-821X(02)01042-7.

Burchfiel, B.C., Quidong, D., Molnar, P., Royden, L., Yipeng, W., Peizhen, Z., and Weiqi, Z., 1989, Intracrustal detachment within zones of continental deformation: Geology, v. 17, no. 8, p. 748–752, https://doi.org/10.1130/0091-7613(1989)017<0448:IDWZOC>2.3.CO;2.

Burchfiel, B.C., Zhang, P., Wang, Y., Zhang, W., Song, F., Deng, Q., Molnar, P., and Royden, L., 1991, Geology of the Haiyuan fault zone, Ningxia-Hui Autonomous Region, China, and its relation to the evolution of the northeastern margin of the Tibetan Plateau: Tectonics, v. 10, no. 6, p. 1091–1110, https://doi.org/10.1029/90TC02685.

Burchfiel, B.C., Zhiliang, C., Yupinc, L., and Royden, L.H., 1995, Tectonics of the Longmen Shan and adjacent regions, central China: International Geology Review, v. 37, no. 8, p. 661–735, https://doi.org/10.1080/00206819509465424.

Burg, J.P., Davy, P., and Martinod, J., 1994, Shortening of analogue models of the continental lithosphere: New hypothesis for the formation of the Tibetan Plateau: Tectonics, v. 13, no. 2, p. 475–483, https://doi.org/10.1029/93TC02738.

Burgess, W.P., Yin, A., Dubey, C.S., Shen, Z.K., and Kelty, T.K., 2012, Holocene shortening across the Main Frontal Thrust zone in the eastern Himalaya: Earth and Planetary Science Letters, v. 357, p. 152–167.

Capitanio, F.A., Morra, G., Goes, S., Weinberg, R.F., and Moresi, L., 2010, India-Asia convergence driven by the subduction of the Greater Indian continent: Nature Geoscience, v. 3, no. 2, p. 136–139, https://doi.org/10.1038/ngeo725.

Champagnac, J.D., Yuan, D.Y., Ge, W.P., Molnar, P., and Zheng, W.J., 2010, Slip rate at the north-eastern front of the Qilian Shan, China: Terra Nova, v. 22, p. 180–187, https://doi.org/10.1111/j.1365-3121.2010.00932.x.

Chen, L., and Gerya, T.V., 2016, The role of lateral lithospheric strength heterogeneities in orogenic plateau growth: Insights from 3-D thermo-mechanical modeling: Journal of Geophysical Research, v. 121, p. 3118–3138.

Chen, S., Wang, H., Wei, J., Lv, Z., Gan, H., and Jin, S., 2014, Sedimentation of the Lower Cretaceous Xiagou Formation and its response to regional tectonics in the Qingxi Sag, Jiuquan Basin, NW China: Cretaceous Research, v. 47, p. 72–86, https://doi.org/10.1016/j.cretres.2013.11.006.

Chen, X., Yin, A., Gehrels, G.E., Cowgill, E.S., Grove, M., Harrison, T.M., and Wang, X.-F., 2003, Two phases of Mesozoic north-south extension in the eastern Altyn Tagh range, northern Tibetan Plateau: Tectonics, v. 22, 1053, https://doi.org/10.1029/2001TC001336.

Chen, Y., Gilder, S., Halim, N., Cogné, J.P., and Courtillot, V., 2002a, New paleomagnetic constraints on central Asian kinematics: Displacement along the Altyn Tagh fault and rotation of the Qaidam Basin: Tectonics, v. 21, no. 5, 1042, https://doi.org/10.1029/2001TC901030.

Chen, Y., Wu, H., Courtillot, V., and Gilder, S., 2002b, Large N-S convergence at the northern edge of the Tibetan Plateau? New Early Cretaceous paleomagnetic data from Hexi Corridor, NW China: Earth and Planetary Science Letters, v. 201, no. 2, p. 293–307, https://doi.org/10.1016/S0012-821X(02)00722-7.

Cheng, F., Jolivet, M., Fu, S., Zhang, Q., Guan, S., Yu, X., and Guo, Z., 2014, Northward growth of the Qimen Tagh Range: A new model accounting for the late Neogene strike-slip deformation of the SW Qaidam Basin: Tectonophysics, v. 632, p. 32–47, https://doi.org/10.1016/j.tecto.2014.05.034.

Cheng, F., Jolivet, M., Dupont-Nivet, G., Wang, L., Yu, X., and Guo, Z., 2015, Lateral extrusion along the Altyn Tagh fault, Qilian Shan (NE Tibet): Insight from a 3D crustal budget: Terra Nova, v. 27, no. 6, p. 416–425, https://doi.org/10.1111/ter.12173.

Cheng, F., Garzione, C., Jolivet, M., Wang, W., Dong, J., Richter, F., and Guo, Z., 2019, Provenance analysis of the Yumen Basin and northern Qilian Shan: Implications for the pre-collisional paleogeography in the NE Tibetan Plateau and eastern termination of Altyn Tagh fault: Gondwana Research, v. 65, p. 156–171, https://doi.org/10.1016/j.gr.2018.08.009.

Christensen, N.I., and Mooney, W.D., 1995, Seismic velocity structure and composition of the continental crust: A global view: Journal of Geophysical Research–Solid Earth, v. 100, no. B6, p. 9761–9788, https://doi.org/10.1029/95JB00259.

Clark, M.K., and Royden, L.H., 2000, Topographic ooze: Building the eastern margin of Tibet by lower crustal flow: Geology, v. 28, p. 703–706, https://doi.org/10.1130/0091-7613(2000)28<703:TOBTEM>2.0.CO;2.

Clark, M.K., 2012, Continental collision slowing due to viscous mantle lithosphere rather than topography: Nature, v. 483, p. 74–77, https://doi.org/10.1038/nature10848.

Clark, M.K., Farley, K.A., Zheng, D., Wang, Z., and Duvall, A.R., 2010, Early Cenozoic faulting of the northern Tibetan Plateau margin from apatite (U-Th)/He ages: Earth and Planetary Science Letters, v. 296, no. 1–2, p. 78–88, https://doi.org/10.1016/j.epsl.2010.04.051.

Cogné, J.P., Halim, N., Chen, Y., and Courtillot, V., 1999, Resolving the problem of shallow magnetizations of Tertiary age in Asia: Insights from paleomagnetic data from the Qiangtang, Kunlun, and Qaidam blocks (Tibet, China), and a new hypothesis: Journal of Geophysical Research–Solid Earth, v. 104, no. B8, p. 17,715–17,734, https://doi.org/10.1029/1999JB900153.

Collettini, C., Niemeijer, A., Viti, C., and Marone, C., 2009, Fault zone fabric and fault weakness: Nature, v. 462, p. 907–910, https://doi.org/10.1038/nature08585.

Copley, A., Avouac, J.P., and Royer, J.Y., 2010, India-Asia collision and the Cenozoic slowdown of the Indian plate: Implications for the forces driving plate motions: Journal of Geophysical Research–Solid Earth, v. 115, no. B3, B03410, https://doi.org/10.1029/2009JB006634.

Cowgill, E., 2007, Impact of riser reconstructions on estimation of secular variation in rates of strike-slip faulting: Revisiting the Cherchen River site along the Altyn Tagh fault, NW China: Earth and Planetary Science Letters, v. 254, no. 3–4, p. 239–255, https://doi.org/10.1016/j.epsl.2006.09.015.

Craddock, W., Kirby, E., and Zhang, H., 2011, Late Miocene–Pliocene range growth in the interior of the northeastern Tibetan Plateau: Lithosphere, v. 3, no. 6, p. 420–438, https://doi.org/10.1130/L159.1.

Craddock, W.H., Kirby, E., Zhang, H., Clark, M.K., Champagnac, J.D., and Yuan, D., 2014, Rates and style of Cenozoic deformation around the Gonghe Basin, northeastern Tibetan Plateau: Geosphere, v. 10, p. 1255–1282, https://doi.org/10.1130/GES01024.1.

DeCelles, P.G., Robinson, D.M., and Zandt, G., 2002, Implications of shortening in the Himalayan fold-thrust belt for uplift of the Tibetan Plateau: Tectonics, v. 21, no. 6, 1062, https://doi.org/10.1029/2001TC001322.

DeCelles, P.G., Kapp, P., Quade, J., and Gehrels, G.E., 2011, Oligocene–Miocene Kailas basin, southwestern Tibet: Record of postcollisional upper-plate extension in the Indus-Yarlung suture zone: GSA Bulletin, v. 123, no. 7-8, p. 1337–1362.

DeCelles, P.G., Kapp, P., Gehrels, G.E., and Ding, L., 2014, Paleocene–Eocene foreland basin evolution in the Himalaya of southern Tibet and Nepal: Implications for the age of initial India-Asia collision: Tectonics, v. 33, no. 5, p. 824–849, https://doi.org/10.1002/2014TC003522.

Dewey, J.F., and Bird, J.M., 1970, Mountain belts and the new global tectonics: Journal of Geophysical Research, v. 75, no. 14, p. 2625–2647, https://doi.org/10.1029/JB075i014p02625.

Dewey, J.F., and Burke, K.C., 1973, Tibetan, Variscan, and Precambrian basement reactivation: Products of continental collision: The Journal of Geology, v. 81, no. 6, p. 683–692, https://doi.org/10.1086/627920.

Dewey, J.F., Shackleton, R.M., Chengfa, C., and Yiyin, S., 1988, The tectonic evolution of the Tibetan Plateau: Philosophical Transactions of the Royal Society of London, ser. B, Biological Sciences, v. 327, p. 379–413.

Ding, L., Spicer, R.A., Yang, J., Xu, Q., Cai, F., Li, S., Lai, Q., Wang, H., Spicer, T.E.V., Yue, Y., Shukla, A., Srivastava, G., Ali Khan, M., Bera, S., and Mehrotra, R., 2017, Quantifying the rise of the Himalaya orogen and implications for the South Asian monsoon: Geology, v. 45, no. 3, p. 215–218, https://doi.org/10.1130/G38583.1.

Du, D.D., Zhang, C.J., Mughal, M.S., Wang, X.Y., Blaise, D., Gao, J.P., Ma, Y., and Luo, X. 2018, Detrital apatite fission track constraints on Cenozoic tectonic evolution of the northeastern Qinghai-Tibet Plateau, China: Evidence from Cenozoic strata in Lulehe section, northern Qaidam Basin: Journal of Mountain Science, v. 15, no. 3, p. 532–547, https://doi.org/10.1007/s11629-017-4692-5.

Dupont-Nivet, G., Horton, B.K., Butler, R.F., Wang, J., Zhou, J., and Waanders, G.L., 2004, Paleogene clockwise tectonic rotation of the Xining-Lanzhou region, northeastern Tibetan Plateau: Journal of Geophysical Research–Solid Earth, v. 109, no. B4, B04401, https://doi.org/10.1029/2003JB002620.

Dupont-Nivet, G., Krijgsman, W., Langereis, C.G., Abels, H.A., Dai, S., and Fang, X., 2007, Tibetan Plateau aridification linked to global cooling at the Eocene-Oligocene transition: Nature, v. 445, p. 635–638, https://doi.org/10.1038/nature05516.

Dupont-Nivet, G., Hoorn, C., and Konert, M., 2008, Tibetan uplift prior to the Eocene-Oligocene climate transition: Evidence from pollen analysis of the Xining Basin: Geology, v. 36, no. 12, p. 987–990, https://doi.org/10.1130/G25063A.1.

Duvall, A.R., Clark, M.K., van der Pluijm, B.A., and Li, C., 2011, Direct dating of Eocene reverse faulting in northeastern Tibet using Ar-dating of fault clays and low-temperature thermochronometry: Earth and Planetary Science Letters, v. 304, no. 3-4, p. 520–526.

Duvall, A.R., Clark, M.K., Kirby, E., Farley, K.A., Craddock, W.H., Li, C., and Yuan, D.Y., 2013, Low-temperature thermochronometry along the Kunlun and Haiyuan faults, NE Tibetan Plateau: Evidence for kinematic change during late-stage orogenesis: Tectonics, v. 32, no. 5, p. 1190–1211, https://doi.org/10.1002/tect.20072.

England, P., and Houseman, G., 1986, Finite strain calculations of continental deformation: 2. Comparison with the India-Asia collision zone: Journal of Geophysical Research, v. 91, no. B3, p. 3664–3676, https://doi.org/10.1029/JB091iB03p03664.

England, P., and Houseman, G., 1989, Extension during continental convergence, with application to the Tibetan Plateau: Journal of Geophysical Research–Solid Earth, v. 94, no. B12, p. 17,561–17,579, https://doi.org/10.1029/JB094iB12p17561.

England, P., and Molnar, P., 1997, Active deformation of Asia: From kinematics to dynamics: Science, v. 278, no. 5338, p. 647–650, https://doi.org/10.1126/science.278.5338.647.

Fang, X., Liu, D., Song, C., Dai, S., and Meng, Q., 2012, Oligocene slow and Miocene–Quaternary rapid deformation and uplift of the Yumu Shan and North Qilian Shan: Evidence from high-resolution magnetostratigraphy and tectonosedimentology, *in* Jovane, L., Herrero-Bervera, E., Hinnov, L.A., and Housen, B., eds., Magnetic Methods and the Timing of Geological Processes: Geological Society, London, Special Publication 373, p. 149–171.

Feng, M., Kumar, P., Mechie, J., Zhao, W., Kind, R., Su, H., Xue, G., Shi, D., and Qian, H., 2014, Structure of the crust and mantle down to 700 km depth beneath the East Qaidam basin and Qilian Shan from P and S receiver functions: Geophysical Journal International, v. 199, p. 1416–1429, https://doi.org/10.1093/gji/ggu335.

Frost, G.M., Coe, R.S., Meng, Z., Peng, Z., Chen, Y., Courtillot, V., Peltzer, G., Tapponnier, P., and Avouac, J.-P., 1995, Preliminary Early Cretaceous paleomagnetic results from the Gansu Corridor, China: Earth and Planetary Science Letters, v. 129, no. 1, p. 217–232, https://doi.org/10.1016/0012-821X(94)00244-S.

Gan, W., Zhang, P., Shen, Z.K., Niu, Z., Wang, M., Wan, Y., et al., 2007, Present-day crustal motion within the Tibetan Plateau inferred from GPS measurements: Journal of Geophysical Research–Solid Earth, v. 112, no. B8, B08416, https://doi.org/10.1029/2005JB004120.

Gansu Geological Bureau, 1989, Regional Geology of Gansu Province: Beijing, Geological Publishing House, 692 p. [in Chinese].

Gao, R., Cheng, X., and Wu, G., 1999, Lithospheric structure and geodynamic model of the Golmud-Ejn transect in northern Tibet, *in* Macfarlane, A., Sorkhabi, R.B., and Quade, J., eds., Himalaya and Tibet: Mountain Roots to Mountain Tops: Geological Society of America Special Paper 328, p. 9–17.

Gao, R., Wang, H., Yin, A., Dong, S., Kuang, Z., Zuza, A.V., Li, W., and Xiong, X., 2013, Tectonic development of the northeastern Tibetan Plateau as constrained by high-resolution deep seismic-reflection data: Lithosphere, v. 5, no. 6, p. 555–574, https://doi.org/10.1130/L293.1.

Gao, R., Lu, Z., Klemperer, S.L., Wang, H., Dong, S., Li, W., and Li, H., 2016, Crustal-scale duplexing beneath the Yarlung Zangbo suture in the western Himalaya: Nature Geoscience, v. 9, no. 7, p. 555–560, https://doi.org/10.1038/ngeo2730.

Gaudemer, Y., Tapponnier, P., Meyer, B., Peltzer, G., Shunmin, G., Zhitai, C., Huagung, D., and Cifuentes, I., 1995, Partitioning of crustal slip between linked, active faults in the eastern Qilian Shan, and evidence for a major seismic gap, the 'Tianzhu gap,' on the western Haiyuan fault, Gansu (China): Geophysical Journal International, v. 120, p. 599–645, https://doi.org/10.1111/j.1365-246X.1995.tb01842.x.

Gehrels, G.E., Yin, A., and Wang, X.F., 2003a, Detrital zircon geochronology of the northeastern Tibetan Plateau: Geological Society of America Bulletin, v. 115, p. 881–896, https://doi.org/10.1130/0016-7606(2003)115<0881:DGOTNT>2.0.CO;2.

Gehrels, G.E., Yin, A., and Wang, X.F., 2003b, Magmatic history of the Altyn Tagh, Nan Shan, and Qilian Shan region of western China: Journal of Geophysical Research, v. 108, 2423, https://doi.org/10.1029/2002JB001876.

George, A.D., Marshallsea, S.J., Wyrwoll, K.H., Jie, C., and Yanchou, L., 2001, Miocene cooling in the northern Qilian Shan, northeastern margin of the Tibetan Plateau, revealed by apatite fission-track and vitrinite-reflectance analysis: Geology, v. 29, no. 10, p. 939–942.

Guo, X., Gao, R., Li, S., Xu, X., Huang, X., Wang, H., Li, W., Zhao, S., and Li, X., 2016, Lithospheric architecture and deformation of NE Tibet: New insights on the interplay of regional tectonic processes: Earth and Planetary Science Letters, v. 449, p. 89–95, https://doi.org/10.1016/j.epsl.2016.05.045.

Halim, N., Cogné, J.P., Chen, Y., Atasiei, R., Besse, J., Courtillot, V., Gilder, S., Marcoux, J., and Zhao, R. L., 1998, New Cretaceous and Early Tertiary paleomagnetic results from Xining-Lanzhou basin, Kunlun and Qiangtang blocks, China: Implications on the geodynamic evolution of Asia: Journal of Geophysical Research–Solid Earth, v. 103, no. B9, p. 21,025–21,045, https://doi.org/10.1029/98JB01118.

Halim, N., Chen, Y., and Cogné, J.P., 2003, A first palaeomagnetic study of Jurassic formations from the Qaidam basin, northeastern Tibet, China—Tectonic implications: Geophysical Journal International, v. 153, no. 1, p. 20–26, https://doi.org/10.1046/j.1365-246X.2003.01860.x.

Haproff, P.J., Zuza, A.V., and Yin, A., 2018, West-directed thrusting south of the eastern Himalayan syntaxis indicates clockwise crustal flow at the indenter corner during the India-Asia collision: Tectonophysics, v. 722, p. 277–285, https://doi.org/10.1016/j.tecto.2017.11.001.

Harrison, T.M., Copeland, P., Kidd, W.S.F., and Yin, A., 1992, Raising Tibet: Science, v. 255, no. 5052, p. 1663–1670.

Hijmans, R.J., Cameron, S.E., Parra, J.L., Jones, P.G., and Jarvis, A., 2005, Very high resolution interpolated climate surfaces for global land areas: International Journal of Climatology, v. 25, p. 1965–1978, https://doi.org/10.1002/joc.1276.

Horton, B.K., Dupont-Nivet, G., Zhou, J., Waanders, G.L., Butler, R.F., and Wang, J., 2004, Mesozoic–Cenozoic evolution of the Xining-Minhe and Dangchang basins, northeastern Tibetan Plateau: Magnetostratigraphic and biostratigraphic results: Journal of Geophysical Research–Solid Earth, v. 109, no. B4, B04402, https://doi.org/10.1029/2003JB002913.

Hu, X., Garzanti, E., Moore, T., and Raffi, I., 2015, Direct stratigraphic dating of India-Asia collision onset at the Selandian (middle Paleocene, 59 ± 1 Ma): Geology, v. 43, no. 10, p. 859–862, https://doi.org/10.1130/G36872.1.

Hu, X., Garzanti, E., Wang, J., Huang, W., An, W., and Webb, A., 2016, The timing of India-Asia collision onset—Facts, theories, controversies: Earth-Science Reviews, v. 160, p. 264–299, https://doi.org/10.1016/j.earscirev.2016.07.014.

Hu, X., Pan, B., Fan, Y., Wang, J., Hu, Z., Cao, B., Li, Q., and Geng, H., 2017, Folded fluvial terraces in a young, actively deforming intramontane basin between the Yumu Shan and the Qilian Shan mountains, NE Tibet: Lithosphere, v. 9, no. 4, p. 545–560, https://doi.org/10.1130/L614.1.

Huang, Z., Tilmann, F., Xu, M., Wang, L., Ding, Z., Mi, N., Yu, D., and Li, H., 2017, Insight into NE Tibetan Plateau expansion from crustal and upper mantle anisotropy revealed by shear-wave splitting: Earth and Planetary Science Letters, v. 478, p. 66–75, https://doi.org/10.1016/j.epsl.2017.08.030.

Huo, Y.L., and Tan, S.D., 1995, Exploration Case History and Petroleum Geology in Jiuquan Continental Basin: Beijing, China, Petroleum Industry Press, 211 p.

Ingalls, M., Rowley, D.B., Currie, B., and Colman, A.S., 2016, Large-scale subduction of continental crust implied by India-Asia mass-balance calculation: Nature Geoscience, v. 9, no. 11, p. 848–853, https://doi.org/10.1038/ngeo2806.

Jesmok, G., Upadhyay, D., Jian, X., Herron-Rutland, M., and Tripati, A., 2018, Temperature measurements and paleoclimate analyses of sedimentary carbonates from the Cenozoic Qaidam Basin, Qinghai Province, China, using stable isotopes and clumped isotope thermometry: Geological Society of America Abstracts with Programs, v. 50, no. 6, paper 197-16.

Ji, J., Zhang, K., Clift, P.D., Zhuang, G., Song, B., Ke, X., and Xu, Y., 2017, High-resolution magnetostratigraphic study of the Paleogene–Neogene strata in the northern Qaidam Basin: Implications for the growth of the northeastern Tibetan Plateau: Gondwana Research, v. 46, p. 141–155, https://doi.org/10.1016/j.gr.2017.02.015.

Jian, X., Guan, P., Zhang, W., Liang, H., Feng, F., and Fu, L., 2018, Late Cretaceous to early Eocene deformation in the northern Tibetan Plateau: Detrital apatite fission track evidence from northern Qaidam Basin: Gondwana Research, v. 60, p. 94–104, https://doi.org/10.1016/j.gr.2018.04.007.

Johnson, M.R.W., 2002, Shortening budgets and the role of continental subduction during the India-Asia collision: Earth-Science Reviews, v. 59, no. 1–4, p. 101–123, https://doi.org/10.1016/S0012-8252(02)00071-5.

Jolivet, M., Brunel, M., Seward, D., Xu, Z., Yang, J., Roger, F., Tapponnier, P., Malavieille, J., Arnaud, N., and Wu, C., 2001, Mesozoic and Cenozoic tectonics of the northern edge of the Tibetan Plateau: Fission-track constraints: Tectonophysics, v. 343, no. 1–2, p. 111–134, https://doi.org/10.1016/S0040-1951(01)00196-2.

Jolivet, M., Brunel, M., Seward, D., Xu, Z., Yang, J., Malavieille, J., Roger, F., Leyreloup, A., Arnaud, N., and Wu, C., 2003, Neogene extension and volcanism in the Kunlun fault zone, northern Tibet: New constraints on the age of the Kunlun fault: Tectonics, v. 22, no. 5, 1052, https://doi.org/10.1029/2002TC001428.

Judge, P.A., and Allmendinger, R.W., 2011, Assessing uncertainties in balanced cross sections: Journal of Structural Geology, v. 33, no. 4, p. 458–467, https://doi.org/10.1016/j.jsg.2011.01.006.

Kapp, P., Murphy, M.A., Yin, A., Harrison, T.M., Ding, L., and Guo, J., 2003, Mesozoic and Cenozoic tectonic evolution of the Shiquanhe area of western Tibet: Tectonics, v. 22, no. 4, 1029, https://doi.org/10.1029/2001TC001332.

Kapp, P., DeCelles, P.G., Gehrels, G.E., Heizler, M., and Ding, L., 2007, Geological records of the Lhasa-Qiangtang and Indo-Asian collisions in the Nima area of central Tibet: Geological Society of America Bulletin, v. 119, no. 7–8, p. 917–933, https://doi.org/10.1130/B26033.1.

Kind, R., Yuan, X., Saul, J., Nelson, D., Sobolev, S.V., Mechie, J., Zhao, W., Kosarev, G., Ni, J., Achauer, U., and Jiang, M., 2002, Seismic images of crust and upper mantle beneath Tibet: Evidence for Eurasian plate subduction: Science, v. 298, no. 5596, p. 1219–1221, https://doi.org/10.1126/science.1078115.

Kong, X., Yin, A., and Harrison, T.M., 1997, Evaluating the role of preexisting weaknesses and topographic distributions in the Indo-Asian collision by use of a thin-shell numerical model: Geology, v. 25, no. 6, p. 527–530, https://doi.org/10.1130/0091-7613(1997)025<0527:ETROPW>2.3.CO;2.

Lavé, J., and Avouac, J.P., 2000, Active folding of fluvial terraces across the Siwaliks Hills, Himalayas of central Nepal: Journal of Geophysical Research: Solid Earth, v. 105, no. B3, p. 5735–5770.

Lease, R.O., Burbank, D.W., Zhang, H., Liu, J., and Yuan, D., 2012, Cenozoic shortening budget for the northeastern edge of the Tibetan Plateau: Is lower crustal flow necessary?: Tectonics, v. 31, no. 3, TC3011, https://doi.org/10.1029/2011TC003066.

Li, B., Chen, X., Zuza, A.V., Hu, D., Ding, W., Huang, P., and Xu, S., 2019, Cenozoic cooling history of the North Qilian Shan, northern Tibetan Plateau, and the initiation of the Haiyuan fault: Constraints from apatite- and zircon-fission track thermochronology: Tectonophysics, https://doi.org/10.1016/j.tecto.2018.12.005 (in press).

Li, Y., and Yang, J., 1998, Tectonic geomorphology in the Hexi Corridor, north-west China: Basin Research, v. 10, no. 3, p. 345–352.

Liu, M., Mooney, W.D., Li, S., Okaya, N., and Detweiler, S., 2006, Crustal structure of the northeastern margin of the Tibetan Plateau from the Songpan-Ganzi terrane to the Ordos basin: Tectonophysics, v. 420, no. 1–2, p. 253–266, https://doi.org/10.1016/j.tecto.2006.01.025.

Long, S., McQuarrie, N., Tobgay, T., and Grujic, D., 2011, Geometry and crustal shortening of the Himalayan fold-thrust belt, eastern and central Bhutan: Geological Society of America Bulletin, v. 123, no. 7–8, p. 1427–1447, https://doi.org/10.1130/B30203.1.

Lu, H., Wang, E., Shi, X., and Meng, K., 2012, Cenozoic tectonic evolution of the Elashan range and its surroundings, northern Tibetan Plateau, as constrained by paleomagnetism and apatite fission track analyses: Tectonophysics, v. 580, p. 150–161, https://doi.org/10.1016/j.tecto.2012.09.013.

Malavieille, J., 2010, Impact of erosion, sedimentation, and structural heritage on the structure and kinematics of orogenic wedges: Analog models and case studies: GSA Today, v. 20, no. 1, p. 4–10, https://doi.org/10.1130/GSATG48A.1.

McQuarrie, N., and Ehlers, T.A., 2015, Influence of thrust belt geometry and shortening rate on thermochronometer cooling ages: Insights from thermokinematic and erosion modeling of the Bhutan Himalaya: Tectonics, v. 34, p. 1055–1079, https://doi.org/10.1002/2014TC003783.

McQuarrie, N., Robinson, D., Long, S., Tobgay, T., Grujic, D., Gehrels, G., and Ducea, M., 2008, Preliminary stratigraphic and structural architecture of Bhutan: Implications for the along strike architecture of the Himalayan system: Earth and Planetary Science Letters, v. 272, no. 1–2, p. 105–117, https://doi.org/10.1016/j.epsl.2008.04.030.

Menold, C.A., Manning, C.E., Yin, A., Tropper, P., Chen, X.H., and Wang, X.F., 2009, Metamorphic evolution, mineral chemistry and thermobarometry of orthogneiss hosting ultrahigh-pressure eclogites in the North Qaidam metamorphic belt, western China: Journal of Asian Earth Sciences, v. 35, no. 3–4, p. 273–284, https://doi.org/10.1016/j.jseaes.2008.12.008.

Menold, C.A., Grove, M., Sievers, N.E., Manning, C.E., Yin, A., Young, E.D., and Ziegler, K., 2016, Argon, oxygen, and boron isotopic evidence documenting $^{40}Ar_E$ accumulation in phengite during water-rich high-pressure subduction metasomatism of continental crust: Earth and Planetary Science Letters, v. 446, p. 56–67, https://doi.org/10.1016/j.epsl.2016.04.010.

Meyer, B., Tapponnier, P., Bourjot, L., Metivier, F., Gaudemer, Y., Peltzer, G., Shunmin, G., and Zhitai, C., 1998, Crustal thickening in Gansu-Qinghai, lithospheric mantle subduction, and oblique, strike-slip controlled growth of the Tibet plateau: Geophysical Journal International, v. 135, no. 1, p. 1–47, https://doi.org/10.1046/j.1365-246X.1998.00567.x.

Mock, C., Arnaud, N.O., and Cantagrel, J.M., 1999, An early unroofing in northeastern Tibet? Constraints from $^{40}Ar/^{39}Ar$ thermochronology on granitoids from the eastern Kunlun range (Qianghai, NW China): Earth and Planetary Science Letters, v. 171, no. 1, p. 107–122, https://doi.org/10.1016/S0012-821X(99)00133-8.

Molnar, P., 1988, Continental tectonics in the aftermath of plate tectonics: Nature, v. 335, p. 131–137, https://doi.org/10.1038/335131a0.

Molnar, P., and Stock, J.M., 2009, Slowing of India's convergence with Eurasia since 20 Ma and its implications for Tibetan mantle dynamics: Tectonics, v. 28, no. 3, TC3001, https://doi.org/10.1029/2008TC002271.

Molnar, P., and Tapponnier, P., 1975, Cenozoic tectonics of Asia: Effects of a continental collision: Science, v. 189, no. 4201, p. 419–426, https://doi.org/10.1126/science.189.4201.419.

Molnar, P., England, P., and Martinod, J., 1993, Mantle dynamics, uplift of the Tibetan Plateau, and the Indian monsoon: Reviews of Geophysics, v. 31, no. 4, p. 357–396, https://doi.org/10.1029/93RG02030.

Mouthereau, F., Watts, A.B., and Burov, E., 2013, Structure of orogenic belts controlled by lithosphere age: Nature Geoscience, v. 6, p. 785–789, https://doi.org/10.1038/ngeo1902.

Murphy, M.A., Yin, A., Harrison, T.M., Dürr, S.B., Chen, Z., Ryerson, F.J., Kidd, S.F., Wang, X., and Zhou, X., 1997, Did the Indo-Asian collision alone create the Tibetan Plateau?: Geology, v. 25, no. 8, p. 719–722, https://doi.org/10.1130/0091-7613(1997)025<0719:DTIACA>2.3.CO;2.

Nábělek, J., Hetényi, G., Vergne, J., Sapkota, S., Kafle, B., Jiang, M., Su, H., Chen, J., Huang, B., and the Hi-CLIMB Team, 2009, Underplating in the Himalaya-Tibet collision zone revealed by the Hi-CLIMB experiment: Science, v. 325, no. 5946, p. 1371–1374, https://doi.org/10.1126/science.1167719.

Pan, G., Ding, J., Yao, D., and Wang, L., 2004, Geological Map of Qinghai-Xiang (Tibet) Plateau and Adjacent Areas: Chengdu, China, Chengdu Institute of Geology and Mineral Resources, China Geological Survey, Chengdu Cartographic Publishing House, scale 1:1,500,000.

Pan, S., and Niu, F., 2011, Large contrasts in crustal structure and composition between the Ordos Plateau and the NE Tibetan Plateau from receiver function analysis: Earth and Planetary Science Letters, v. 303, no. 3, p. 291–298, https://doi.org/10.1016/j.epsl.2011.01.007.

Powell, C.M.A., and Conaghan, P.J., 1973, Polyphase deformation in Phanerozoic rocks of the Central Himalayan Gneiss, northwest India: The Journal of Geology, v. 81, p. 127–143, https://doi.org/10.1086/627830.

Priestley, K., and McKenzie, D., 2013, The relationship between shear wave velocity, temperature, attenuation and viscosity in the shallow part of the mantle: Earth and Planetary Science Letters, v. 381, p. 78–91, https://doi.org/10.1016/j.epsl.2013.08.022.

Pullen, A., Kapp, P., Gehrels, G.E., Vervoort, J.D., and Ding, L., 2008, Triassic continental subduction in central Tibet and Mediterranean-style closure of the Paleo-Tethys Ocean: Geology, v. 36, no. 5, p. 351–354, https://doi.org/10.1130/G24435A.1.

Qi, B., Hu, D., Yang, X., Zhang, Y., Tan, C., Zhang, P., and Feng, C., 2016, Apatite fission track evidence for the Cretaceous–Cenozoic cooling history of the Qilian Shan (NW China) and for stepwise northeastward growth of the northeastern Tibetan Plateau since early Eocene: Journal of Asian Earth Sciences, v. 124, p. 28–41, https://doi.org/10.1016/j.jseaes.2016.04.009.

Qinghai Bureau of Geology and Mineral Resources (BGMR), 1991, Regional Geology of Qinghai Province: Beijing, Geological Publishing House, 662 p.

Reith, R.C., 2013, Structural Geology of a Central Segment of the Qilian Shan–Nan Shan Thrust Belt: Implications for the Magnitude of Cenozoic Shortening in the Northeastern Tibetan Plateau [M.S. thesis]: Los Angeles, California, University of California, 73 p.

Robinson, D.M., DeCelles, P.G., and Copeland, P., 2006, Tectonic evolution of the Himalayan thrust belt in western Nepal: Implications for channel flow models: Geological Society of America Bulletin, v. 118, no. 7–8, p. 865–885, https://doi.org/10.1130/B25911.1.

Robinson, P.T., Bai, W.J., Malpas, J., Yang, J.S., Zhou, M.F., Fang, Q.S., Hu, X., Cameron, S., and Staudigel, H., 2004, Ultra-high pressure minerals in the Luobusa Ophiolite, Tibet, and their tectonic implications, *in* Malpas, J., Fletcher, C.J.N., Ali, J.R., and Aitchison, J.C., eds., Aspects of the Tectonic Evolution of China: Geological Society, London, Special Publication 226, p. 247–271, https://doi.org/10.1144/GSL.SP.2004.226.01.14.

Royden, L.H., Burchfiel, B.C., King, R.W., Wang, E., Chen, Z., Shen, F., and Liu, Y., 1997, Surface deformation and lower crustal flow in eastern Tibet: Science, v. 276, no. 5313, p. 788–790, https://doi.org/10.1126/science.276.5313.788.

Royden, L.H., Burchfiel, B.C., and van der Hilst, R.D., 2008, The geological evolution of the Tibetan Plateau: Science, v. 321, no. 5892, p. 1054–1058, https://doi.org/10.1126/science.1155371.

Schulte-Pelkum, V., Monsalve, G., Sheehan, A., Pandey, M.R., Sapkota, S., Bilham, R., and Wu, F., 2005, Imaging the Indian subcontinent beneath the Himalaya: Nature, v. 435, p. 1222–1225, https://doi.org/10.1038/nature03678.

Sobel, E.R., and Arnaud, N., 1999, A possible middle Paleozoic suture in the Altyn Tagh, NW China: Tectonics, v. 18, no. 1, p. 64–74, https://doi.org/10.1029/1998TC900023.

Song, B., Zhang, K., Zhang, L., Ji, J., Hong, H., Wei, Y., Xu, Y., Algeo, T.J., and Wang, C., 2018, Qaidam Basin paleosols reflect climate and weathering intensity on the northeastern Tibetan Plateau during the early Eocene climatic optimum: Palaeogeography, Palaeoclimatology, Palaeoecology, https://doi.org/10.1016/j.palaeo.2018.03.027 (in press).

Song, S., Niu, Y., Su, L., and Xia, X., 2013, Tectonics of the North Qilian orogen, NW China: Gondwana Research, v. 23, no. 4, p. 1378–1401, https://doi.org/10.1016/j.gr.2012.02.004.

Song, S.G., and Su, L., 1998, Plastic rheology of the Yushigou mantle peridotite and implications for dynamics of paleo-plate movement in the North Qilian Mountains: Acta Geologica Sinica (English edition), v. 72, p. 131–141.

Song, S.G., Zhang, L.F., Niu, Y., Wei, C.J., Liou, J.G., and Shu, G.M., 2007, Eclogite and carpholite-bearing metasedimentary rocks in the North Qilian suture zone, NW China: Implications for early Palaeozoic cold oceanic subduction and water transport into mantle: Journal of Metamorphic Geology, v. 25, no. 5, p. 547–563, https://doi.org/10.1111/j.1525-1314.2007.00713.x.

Song, S.G., Niu, Y., Zhang, L.F., Wei, C.J., Liou, J.G., and Su, L., 2009, Tectonic evolution of early Paleozoic HP metamorphic rocks in the North Qilian Mountains, NW China: New perspectives: Journal of Asian Earth Sciences, v. 35, p. 334–353, https://doi.org/10.1016/j.jseaes.2008.11.005.

Song, S., Niu, Y., Su, L., Zhang, C., and Zhang, L., 2014, Continental orogenesis from ocean subduction, continent collision/subduction, to orogen collapse, and orogen recycling: The example of the North Qaidam UHPM belt, NW China: Earth-Science Reviews, v. 129, p. 59–84.

Styron, R., Taylor, M., and Sundell, K., 2015, Accelerated extension of Tibet linked to the northward underthrusting of Indian crust: Nature Geoscience, v. 8, no. 2, p. 131–134, https://doi.org/10.1038/ngeo2336.

Sun, Z.M., Yang, Z.Y., Pei, J.L., Yang, T.S., and Wang, X.S., 2006, New Early Cretaceous paleomagnetic data from volcanic and red beds of the eastern Qaidam block and its implications for tectonics of Central Asia: Earth and Planetary Science Letters, v. 243, p. 268–281, https://doi.org/10.1016/j.epsl.2005.12.016.

Tapponnier, P., Peltzer, G., Le Dain, A.Y., Armijo, R., and Cobbold, P., 1982, Propagating extrusion tectonics in Asia: New insights from simple experiments with plasticine: Geology, v. 10, no. 12, p. 611–616, https://doi.org/10.1130/0091-7613(1982)10<611:PETIAN>2.0.CO;2.

Tapponnier, P., Meyer, B., Avouac, J.P., Peltzer, G., Gaudemer, Y., Guo, S., Xiang, H., Yin, K., Chen, Z., Cai, S., and Dai, H., 1990, Active thrusting and folding in the Qilian Shan, and decoupling between upper crust and mantle in northeastern Tibet: Earth and Planetary Science Letters, v. 97, p. 382–403, https://doi.org/10.1016/0012-821X(90)90053-Z.

Tapponnier, P., Zhiqin, X., Roger, F., Meyer, B., Arnaud, N., Wittlinger, G., and Jingsui, Y., 2001, Oblique stepwise rise and growth of the Tibet Plateau: Science, v. 294, no. 5547, p. 1671–1677, https://doi.org/10.1126/science.105978.

Taylor, M., and Yin, A., 2009, Active structures of the Himalayan-Tibetan orogen and their relationships to earthquake distribution, contemporary strain field, and Cenozoic volcanism: Geosphere, v. 5, no. 3, p. 199–214, https://doi.org/10.1130/GES00217.1.

Thiede, R.C., and Ehlers, T.A., 2013, Large spatial and temporal variations in Himalayan denudation: Earth and Planetary Science Letters, v. 371, p. 278–293, https://doi.org/10.1016/j.epsl.2013.03.004.

Tian, X., Liu, Z., Si, S., and Zhang, Z., 2014, The crustal thickness of NE Tibet and its implication for crustal shortening: Tectonophysics, v. 634, p. 198–207, https://doi.org/10.1016/j.tecto.2014.07.001.

Tian, Y., Kohn, B., Philipps, D., Hu, S., Gleadow, A.J.W., and Carter, A., 2016, Late Cretaceous–earliest Paleogene deformation in the Longmen Shan fold-and-thrust belt, eastern Tibetan Plateau margin: Pre-Cenozoic thickened crust?: Tectonics, v. 35, p. 2293–2312, https://doi.org/10.1002/2016TC004182.

van Hinsbergen, D.J., Kapp, P., Dupont-Nivet, G., Lippert, P.C., DeCelles, P.G., and Torsvik, T.H., 2011a, Restoration of Cenozoic deformation in Asia and the size of Greater India: Tectonics, v. 30, no. 5, TC5003, https://doi.org/10.1029/2011TC002908.

van Hinsbergen, D.J., Steinberger, B., Doubrovine, P.V., and Gassmöller, R., 2011b, Acceleration and deceleration of India-Asia convergence since the Cretaceous: Roles of mantle plumes and continental collision: Journal of Geophysical Research–Solid Earth, v. 116, no. B6, B06101, https://doi.org/10.1029/2010JB008051.

Vincent, S.J., and Allen, M.B., 1999, Evolution of the Minle and Chaoshui Basins, China: Implications for Mesozoic strike-slip basin formation in Central Asia: Geological Society of America Bulletin, v. 111, no. 5, p. 725–742, https://doi.org/10.1130/0016-7606(1999)111<0725:EOTMAC>2.3.CO;2.

Wallis, S., Tsujimori, T., Aoya, M., Kawakami, T., Terada, K., Suzuki, K., and Hyodo, H., 2003, Cenozoic and Mesozoic metamorphism in the Longmenshan orogen: Implications for geodynamic models of eastern Tibet: Geology, v. 31, no. 9, p. 745–748, https://doi.org/10.1130/G19562.1.

Wang, C., Zhao, X., Liu, Z., Lippert, P.C., Graham, S.A., Coe, R.S., Yi, H., Zhu, L., Liu, S., and Li, Y., 2008, Constraints on the early uplift history of the Tibetan Plateau: Proceedings of the National Academy of Sciences of the United States of America, v. 105, no. 13, p. 4987–4992, https://doi.org/10.1073/pnas.0703595105.

Wang, C., Gao, R., Yin, A., Wang, H., Zhang, Y., Guo, T., Li, Q., and Li, Y., 2011, A mid-crustal strain-transfer model for continental deformation: A new perspective from high-resolution deep seismic-reflection profiling across NE Tibet: Earth and Planetary Science Letters, v. 306, no. 3–4, p. 279–288, https://doi.org/10.1016/j.epsl.2011.04.010.

Wang, E., and Burchfiel, B.C., 2004, Late Cenozoic right-lateral movement along the Wenquan fault and associated deformation: Implications for the kinematic history of the Qaidam Basin, northeastern Tibetan Plateau: International Geology Review, v. 46, no. 10, p. 861–879, https://doi.org/10.2747/0020-6814.46.10.861.

Wang, Q., and Liu, X.Y., 1981, On Caledonian polycyclic paired metamorphic belts of Qilian Mountains, northwest China, *in* Huang, T.K., and Li, C.Y., eds., Contributions to Tectonics of China and Adjacent Regions: Beijing, Geological Publishing House, p. 92–101 [in Chinese with English abstract].

Wang, W., Zheng, W., Zhang, P., Li, Q., Kirby, E., Yuan, D., Zheng, D., Liu, C., Wang, Z., Zhang, H., and Pang, J., 2017, Expansion of the Tibetan Plateau during the Neogene: Nature Communications, v. 8, article 15887, https://doi.org/10.1038/ncomms15887.

Wang, X., Wang, B., Qiu, Z., Xie, G., Xie, J., Downs, W., Qiu, Z., and Deng, T., 2003, Danghe area (western Gansu, China) biostratigraphy and implications in depositional history and tectonics of the northern Tibetan Plateau: Earth and Planetary Science Letters, v. 208, p. 253–269, https://doi.org/10.1016/S0012-821X(03)00047-5.

Webb, A.A.G., 2013, Preliminary balanced palinspastic reconstruction of Cenozoic deformation across the Himachal Himalaya (northwestern India): Geosphere, v. 9, no. 3, p. 572–587, https://doi.org/10.1130/GES00787.1.

Webb, A.A.G., Yin, A., Harrison, T.M., Célérier, J., Gehrels, G.E., Manning, C.E., and Grove, M., 2011, Cenozoic tectonic history of the Himachal Himalaya (northwestern India) and its constraints on the formation mechanism of the Himalayan orogen: Geosphere, v. 7, p. 1013–1061, https://doi.org/10.1130/GES00627.1.

Webb, A.A.G., Guo, H., Clift, P.D., Husson, L., Müller, T., Costantino, D., Yin, A., Xu, Z., Cao, H., and Wang, Q., 2017, The Himalaya in 3D: Slab dynamics controlled mountain building and monsoon intensification: Lithosphere, v. 9, no. 4, p. 637–651, https://doi.org/10.1130/L636.1.

Wei, X., Jiang, M., Liang, X., Chen, L., and Ai, Y., 2017, Limited southward underthrusting of the Asian lithosphere and material extrusion beneath the northeastern margin of Tibet, inferred from teleseismic Rayleigh wave tomography: Journal of Geophysical Research–Solid Earth, v. 122, no. 9, p. 7172–7189, https://doi.org/10.1002/2016JB013832.

Wei, Y., Xiao, A., Wu, L., Mao, L., Zhao, H., Shen, Y., and Wang, L., 2016, Temporal and spatial patterns of Cenozoic deformation across the Qaidam Basin, northern Tibetan Plateau: Terra Nova, v. 28, no. 6, p. 409–418, https://doi.org/10.1111/ter.12234.

Whipple, K.X., and Meade, B.J., 2004, Controls on the strength of coupling among climate, erosion, and deformation in two-sided, frictional orogenic wedges at steady state: Journal of Geophysical Research, v. 109, F01011, https://doi.org/10.1029/2003JF000019.

Willett, S.D., 1999, Orogeny and orography: The effects of erosion on the structure of mountain belts: Journal of Geophysical Research, v. 104, no. B12, p. 28,957–28,981, https://doi.org/10.1029/1999JB900248.

Willett, S.D., and Beaumont, C., 1994, Subduction of Asian lithospheric mantle beneath Tibet inferred from models of continental collision: Nature, v. 369, p. 642–645, https://doi.org/10.1038/369642a0.

Worley, B.A., and Wilson, C.J., 1996, Deformation partitioning and foliation reactivation during transpressional orogenesis, an example from the central Longmen Shan, China: Journal of Structural Geology, v. 18, no. 4, p. 395–411, https://doi.org/10.1016/0191-8141(95)00095-U.

Wu, C., Yin, A., Zuza, A.V., Zhang, J., Liu, W., and Ding, L., 2016, Pre-Cenozoic geologic history of the central and northern Tibetan Plateau and the role of Wilson cycles in constructing the Tethyan orogenic system: Lithosphere, v. 8, no. 3, p. 254–292, https://doi.org/10.1130/L494.1.

Wu, C., Zuza, A.V., Yin, A., Liu, C., Reith, R.C., Zhang, J., Liu, W., and Zhou, Z., 2017, Geochronology and geochemistry of Neoproterozoic granitoids in the central Qilian Shan of northern Tibet: Reconstructing the amalgamation processes and tectonic history of Asia: Lithosphere, v. 9, no. 4, p. 609–636, https://doi.org/10.1130/L640.1.

Xia, X.H., and Song, S.G., 2010, Forming age and tectono-petrogenesis of the Jiugequan ophiolite in the North Qilian Mountain, NW China: Chinese Science Bulletin, v. 55, p. 1899–1907, https://doi.org/10.1007/s11434-010-3207-3.

Xiang, Z.Q., Lu, S.N., Li, H.K., Li, H.M., Song, B., and Zheng, J.K., 2007, SHRIMP U-Pb zircon age of gabbro in Aoyougou in the western segment of the North Qilian Mountains, China, and its geological implications: Geological Bulletin of China, v. 26, p. 1686–1691.

Xiao, W., Windley, B.F., Yong, Y., Yan, Z., Yuan, C., Liu, C., and Li, J., 2009, Early Paleozoic to Devonian multiple-accretionary model for the Qilian Shan, NW China: Journal of Asian Earth Sciences, v. 35, no. 3, p. 323–333, https://doi.org/10.1016/j.jseaes.2008.10.001.

Xiao, X.C., Chen, G.M., and Zhu, Z.Z., 1974, Some knowledge about the paleo-plate tectonics of the Qilian Mountains: Geological Science and Technology, v. 3, p. 73–78 [in Chinese with English abstract].

Xu, X., Niu, F., Ding, Z., and Chen, Q., 2018, Complicated crustal deformation beneath the NE margin of the Tibetan Plateau and its adjacent areas revealed by multi-station receiver-function gathering: Earth and Planetary Science Letters, v. 497, p. 204–216, https://doi.org/10.1016/j.epsl.2018.06.010.

Yakovlev, P.V., and Clark, M.K., 2014, Conservation and redistribution of crust during the Indo-Asian collision: Tectonics, v. 33, no. 6, p. 1016–1027, https://doi.org/10.1002/2013TC003469.

Yang, H., Yang, X., Zhang, H., Huang, X., Huang, W., and Zhang, N., 2018, Active fold deformation and crustal shortening rates of the Qilian Shan foreland thrust belt, NE Tibet, since the late Pleistocene: Tectonophysics, v. 742–743, p. 84–100, https://doi.org/10.1016/j.tecto.2018.05.019.

Yang, S., Cheng, X., Xiao, A., Chen, J., Fan, M., and Tain, D., 2007, The structural characteristics of northern Qilian Shan Mountain thrust belt and its control on the oil and gas accumulation: Beijing, Science Press, p. 70–82 [in Chinese].

Ye, Z., Gao, R., Li, Q., Zhang, H., Shen, X., Liu, X., and Gong, C., 2015, Seismic evidence for the North China plate underthrusting beneath northeastern Tibet and its implications for plateau growth: Earth and Planetary Science Letters, v. 426, p. 109–117, https://doi.org/10.1016/j.epsl.2015.06.024.

Yin, A., 2010, Cenozoic tectonic evolution of Asia: A preliminary synthesis: Tectonophysics, v. 488, no. 1–4, p. 293–325, https://doi.org/10.1016/j.tecto.2009.06.002.

Yin, A., and Harrison, T.M., 2000, Geologic evolution of the Himalayan-Tibetan orogen: Annual Review of Earth and Planetary Sciences, v. 28, no. 1, p. 211–280, https://doi.org/10.1146/annurev.earth.28.1.211.

Yin, A., Rumelhart, P.E., Butler, R., Cowgill, E., Harrison, T.M., Foster, D.A., Ingersoll, R.V., Qing, Z., Xian-Qiang, Z., Xiao-Feng, W., Hanson, A., and Raza, A., 2002, Tectonic history of the Altyn Tagh fault system in northern Tibet inferred from Cenozoic sedimentation: Geological Society of America Bulletin, v. 114, no. 10, p. 1257–1295, https://doi.org/10.1130/0016-7606(2002)114<1257:THOTAT>2.0.CO;2.

Yin, A., Dang, Y.-Q., Zhang, M., McRivette, M.W., Burgess, W.P., and Chen, X.-H., 2007a, Cenozoic tectonic evolution of Qaidam Basin and its surrounding regions (part 2): Wedge tectonics in southern Qaidam Basin and the Eastern Kunlun Range, *in* Sears, J.W., Harms, T.A., and Evenchick, C.A., eds., Whence the Mountains? Inquiries into the Evolution of Orogenic Systems: A Volume in Honor of Raymond A. Price: Geological Society of America Special Paper 433, p. 369–390, https://doi.org/10.1130/2007.2433(18).

Yin, A., Manning, C.E., Lovera, O., Menold, C.A., Chen, X., and Gehrels, G.E., 2007b, Early Paleozoic tectonic and thermomechanical evolution of ultrahigh-pressure (UHP) metamorphic rocks in the northern Tibetan Plateau, northwest China: International Geology Review, v. 49, p. 681–716, https://doi.org/10.2747/0020-6814.49.8.681.

Yin, A., Dang, Y.-Q., Wang, L.-C., Jiang, W.-M., Zhou, S.-P., Chen, X.-H., Gehrels, G.E., and McRivette, M.W., 2008a, Cenozoic tectonic evolution of Qaidam Basin and its surrounding regions (part 1): The southern Qilian Shan–Nan Shan thrust belt and northern Qaidam Basin: Geological Society of America Bulletin, v. 120, no. 7–8, p. 813–846, https://doi.org/10.1130/B26180.1.

Yin, A., Dang, Y.Q., Zhang, M., Chen, X.H., and McRivette, M.W., 2008b, Cenozoic tectonic evolution of the Qaidam Basin and its surrounding regions (Part 3): Structural geology, sedimentation, and regional tectonic reconstruction: Geological Society of America Bulletin, v. 120, no. 7–8, p. 847–876, https://doi.org/10.1130/B26232.1.

Yin, A., Dubey, C.S., Kelty, T.K., Webb, A.A.G., Harrison, T.M., Chou, C.Y., and Célérier, J., 2010, Geologic correlation of the Himalayan orogen and Indian craton: Part 2. Structural geology, geochronology, and tectonic evolution of the Eastern Himalaya: GSA Bulletin, v. 122, no. 3-4, p. 360–395.

Yu, X., Guo, Z., and Fu, S., 2015, Endorheic or exorheic: Differential isostatic effects of Cenozoic sediments on the elevations of the cratonic basins around the Tibetan Plateau: Terra Nova, v. 27, no. 1, p. 21–27, https://doi.org/10.1111/ter.12126.

Yu, X., Guo, Z., Zhang, Q., Cheng, X., Du, W., Wang, Z., and Bian, Q., 2017, Denan Depression controlled by northeast-directed Olongbulak thrust zone in northeastern Qaidam Basin: Implications for growth of northern Tibetan Plateau: Tectonophysics, v. 717, p. 116–126, https://doi.org/10.1016/j.tecto.2017.06.017.

Yuan, D.Y., Champagnac, J.D., Ge, W.P., Molnar, P., Zhang, P.Z., Zheng, W.J., Zhang, H.P., and Liu, X.W., 2011, Late Quaternary right-lateral slip rates of faults adjacent to Lake Qinghai, northeastern margin of the Tibetan Plateau: Geological Society of America Bulletin, v. 123, no. 9–10, p. 2016–2030, https://doi.org/10.1130/B30315.1.

Yuan, D.Y., Ge, W.P., Chen, Z.W., Li, C.Y., Wang, Z.C., Zhang, H.P., Zhang, P.Z., Zheng, D.W., Zheng, W.J., Craddock, W.H., Dayem, K.E., Duvall, A.R., Hough, B.G., Lease, R.O., Champagnac, J.D., Burbank, D.W., Clark, M.K., Farley, K.A., Garzione, C.N., Kirby, E., Molnar, P., and Roe, G.H., 2013, The growth of northeastern Tibet and its relevance to large-scale continental geodynamics: A review of recent studies: Tectonics, v. 32, no. 5, p. 1358–1370, https://doi.org/10.1002/tect.20081.

Yue, H., Chen, Y.J., Sandvol, E., Ni, J., Hearn, T., Zhou, S., Feng, Y., Ge, Z., Trujillo, A., Wang, Y., Jin, G., Jiang, M., Tang, Y., Liang, X., Wei, S., Wang, H., Fan, W., and Liu, Z., 2012, Lithospheric and upper mantle structure of the northeastern Tibetan Plateau: Journal of Geophysical Research–Solid Earth, v. 117, no. B5, B05307, https://doi.org/10.1029/2011JB008545.

Yue, Y., Ritts, B.D., and Graham, S.A., 2001, Initiation and long-term slip history of the Altyn Tagh fault: International Geology Review, v. 43, no. 12, p. 1087–1093, https://doi.org/10.1080/00206810109465062.

Zhang, H., Zhang, P., Prush, V., Zheng, D., Zheng, W., Wang, W., Liu, C., and Ren, Z., 2017, Tectonic geomorphology of the Qilian Shan in the northeastern Tibetan Plateau: Insights into the plateau formation processes: Tectonophysics, v. 706, p. 103–115, https://doi.org/10.1016/j.tecto.2017.04.016.

Zhang, L.Y., Ding, L., Pullen, A., Xu, Q., Liu, D.L., Cai, F.L., Yue, Y.H., Lai, Q.Z., Shi, R.D., Ducea, M.N., Kapp, P., and Chapman, A., 2014, Age and geochemistry of western Hoh-Xil–Songpan-Ganzi granitoids, northern Tibet: Implications for the Mesozoic closure of the Paleo-Tethys Ocean: Lithos, v. 190, p. 328–348, https://doi.org/10.1016/j.lithos.2013.12.019.

Zhang, P., Burchfiel, B.C., Molnar, P., Zhang, W., Jiao, D., Deng, Q., Wang, Y., Royden, L., and Song, F., 1991, Amount and style of late Cenozoic deformation in the Liupan Shan area, Ningxia Autonomous Region, China: Tectonics, v. 10, no. 6, p. 1111–1129, https://doi.org/10.1029/90TC02686.

Zhang, P.Z., Shen, Z., Wang, M., Gan, W., Bürgmann, R., Molnar, P., Wang, Q., Niu, Z., Sun, J., Wu, J., Hanrong, S., and Xinzhao, Y., 2004, Continuous deformation of the Tibetan Plateau from global positioning system data: Geology, v. 32, no. 9, p. 809–812, https://doi.org/10.1130/G20554.1.

Zhao, J., Yuan, X., Liu, H., Kumar, P., Pei, S., Kind, R., Zhang, Z., Teng, J., Ding, L., Gao, X., Xu, Q., and Wang, W.,, 2010, The boundary between the Indian and Asian tectonic plates below Tibet: Proceedings of the National Academy of Sciences of the United States of America, v. 107, no. 25, p. 11,229–11,233, https://doi.org/10.1073/pnas.1001921107.

Zhao, W., Mechie, J., Brown, L.D., Guo, J., Haines, S., Hearn, T.M., Klemperer, S.L., Ma, Y.S., Meissner, R., Nelson, K.D., Ni, J.F., Pananont, P., Rapine, R., Ross, A., and Saul, J., 2001, Crustal structure of central Tibet as derived from project INDEPTH wide-angle seismic data: Geophysical Journal International, v. 145, no. 2, p. 486–498, https://doi.org/10.1046/j.0956-540x.2001.01402.x.

Zhao, W., Kumar, P., Mechie, J., Kind, R., Meissner, R., Wu, Z., Shi, D., Su, H., Xue, G., Karplus, M., and Tilmann, F., 2011, Tibetan plate overriding the Asian plate in central and northern Tibet: Nature Geoscience, v. 4, no. 12, p. 870–873, https://doi.org/10.1038/ngeo1309.

Zhao, W.-L., and Morgan, W.J., 1987, Injection of Indian crust into Tibetan lower crust: A two-dimensional finite element model study: Tectonics, v. 6, no. 4, p. 489–504, https://doi.org/10.1029/TC006i004p00489.

Zheng, D., Clark, M.K., Zhang, P., Zheng, W., and Farley, K.A., 2010, Erosion, fault initiation and topographic growth of the North Qilian Shan (northern Tibetan Plateau): Geosphere, v. 6, no. 6, p. 937–941, https://doi.org/10.1130/GES00523.1.

Zheng, D., Wang, W., Wan, J., Yuan, D., Liu, C., Zheng, W., Zhang, H., Pang, J., and Zhang, P., 2017, Progressive northward growth of the northern Qilian Shan–Hexi Corridor (northeastern Tibet) during the Cenozoic: Lithosphere, v. 9, no. 3, p. 408–416, https://doi.org/10.1130/L587.1.

Zhou, H.W., and Murphy, M.A., 2005, Tomographic evidence for wholesale underthrusting of India beneath the entire Tibetan Plateau: Journal of Asian Earth Sciences, v. 25, no. 3, p. 445–457, https://doi.org/10.1016/j.jseaes.2004.04.007.

Zhuang, G., Hourigan, J.K., Ritts, B.D., and Kent-Corson, M.L., 2011, Cenozoic multiple-phase tectonic evolution of the northern Tibetan Plateau: Constraints from sedimentary records from Qaidam Basin, Hexi Corridor, and Subei Basin, northwest China: American Journal of Science, v. 311, no. 2, p. 116–152, https://doi.org/10.2475/02.2011.02.

Zhuang, G., Johnstone, S.A., Hourigan, J., Ritts, B., Robinson, A., and Sobel, E.R., 2018, Understanding the geologic evolution of northern Tibetan Plateau with multiple thermochronometers: Gondwana Research, v. 58, p. 195–210, https://doi.org/10.1016/j.gr.2018.02.014.

Zuza, A.V., and Yin, A., 2016, Continental deformation accommodated by non-rigid passive bookshelf faulting: An example from the Cenozoic tectonic development of northern Tibet: Tectonophysics, v. 677, p. 227–240, https://doi.org/10.1016/j.tecto.2016.04.007.

Zuza, A.V., and Yin, A., 2017, Balkatach hypothesis: A new model for the evolution of the Pacific, Tethyan, and Paleo-Asian oceanic domains: Geosphere, v. 13, no. 5, p. 1664–1712, https://doi.org/10.1130/GES01463.1.

Zuza, A.V., Cheng, X., and Yin, A., 2016a, Testing models of Tibetan Plateau formation with Cenozoic shortening estimates across the Qilian Shan–Nan Shan thrust belt: Geosphere, v. 12, no. 2, p. 501–532, https://doi.org/10.1130/GES01254.1.

Zuza, A.V., Li, B., Tremblay, M.M., Chen, X., Shuster, D.L., and Yin, A., 2016b, Cenozoic development of the northern Tibetan Plateau and the onset of thrust and strike-slip faulting: Constraints from apatite and zircon (U-Th)/He and fission-track thermochronometry: San Francisco, California, American Geophysical Union, Fall Meeting 2016, abstract T11A-2586.

Zuza, A.V., Yin, A., Lin, J., and Sun, M., 2017a, Spacing and strength of active continental strike-slip faults: Earth and Planetary Science Letters, v. 457, p. 49–62.

Zuza, A.V., Levy, D.A., Wang, Z., Xiong, X., and Chen, X., 2017b, Kinematic development of the Tibetan Plateau's northern margin: A traverse across the Qilian Shan–Nan Shan thrust belt: New Orleans, Louisiana, American Geophysical Union, Fall Meeting 2017, abstract T33C-0718.

Zuza, A.V., Wu, C., Reith, R.C., Yin, A., Li, J., Zhang, J., Zhang, Y., Wu, L., and Liu, W., 2018, Tectonic evolution of the Qilian Shan: An early Paleozoic orogen reactivated in the Cenozoic: Geological Society of America Bulletin, v. 130, no. 5–6, p. 881–925, https://doi.org/10.1130/B31721.1.

MANUSCRIPT RECEIVED 26 SEPTEMBER 2018
REVISED MANUSCRIPT RECEIVED 24 OCTOBER 2018
MANUSCRIPT ACCEPTED 3 DECEMBER 2018